

1 NON-CROSSING NONLINEAR REGRESSION
2 QUANTILES BY MONOTONE COMPOSITE QUANTILE
3 REGRESSION NEURAL NETWORK, WITH
4 APPLICATION TO RAINFALL EXTREMES

5 Alex J. Cannon*

Climate Research Division, Environment and Climate Change Canada,
Victoria, British Columbia, Canada

*Corresponding author: Email <alex.cannon@canada.ca>; Phone +1-250-363-8006

Abstract

The goal of quantile regression is to estimate conditional quantiles for specified values of quantile probability using linear or nonlinear regression equations. These estimates are prone to “quantile crossing”, where regression predictions for different quantile probabilities do not increase as probability increases. In the context of the environmental sciences, this might lead to growth curves for an organism where the estimated 80th percentile of weight at a given age exceeds the 90th percentile, or where the estimated magnitude of a 10-yr return period rainstorm exceeds that of a 20-yr storm. This problem, as well as the potential for overfitting, is exacerbated for small to moderate sample sizes and for nonlinear quantile regression models. As a remedy, this study introduces a novel nonlinear quantile regression model, the monotone composite quantile regression neural network (MCQRNN), that (1) simultaneously estimates multiple non-crossing, nonlinear conditional quantile functions; (2) allows for optional monotonicity, positivity/non-negativity, and generalized additive model constraints; and (3) can be adapted to estimate standard least-squares regression and non-crossing expectile regression functions. First, the MCQRNN model is evaluated on synthetic data from multiple functions and error distributions using Monte Carlo simulations. MCQRNN outperforms the benchmark models for non-normal error distributions and reaches the same level of performance as the optimal model for the normal error distribution. Next, the MCQRNN model is applied to real-world climate data by estimating rainfall Intensity-Duration-Frequency (IDF) curves at locations in Canada. IDF curves summarize the relationship between the intensity and occurrence frequency of extreme rainfall over storm durations ranging from minutes to a day. Because annual maximum rainfall intensity is a non-negative quantity that should increase monotonically as the occurrence frequency and storm duration decrease, monotonicity and non-negativity constraints are key constraints in IDF curve estimation. In comparison to standard QRNN models, the ability of the MCQRNN model to incorporate these constraints, in addition to non-crossing, leads to more robust and realistic estimates of extreme rainfall.

1 Introduction

Estimating regression quantiles – conditional quantiles of a response variable that depend on covariates in some form of regression equation – is a fundamental task in data-driven science. Focusing on the environmental sciences, quantile regression methods have been used to provide estimates of predictive uncertainty in forecast applications (Cawley *et al.*, 2007); construct growth curves for organisms (Muggeo *et al.*, 2013); relate soil moisture deficit with summer hot extremes (Hirschi *et al.*, 2010); provide flood frequency estimates (Ouali *et al.*, 2016); estimate rainfall Intensity-Duration-Frequency (IDF) curves (Ouali and Cannon, 2017); determine the relation between rainfall intensity and duration and landslide occurrence (Saito *et al.*, 2010); estimate trends in climate, streamflow, and sea level data (Koenker and Schorfheide, 1994; Barbosa, 2008; Allamano *et al.*, 2009; Roth *et al.*, 2015); downscale atmospheric model outputs (Friederichs and Hense, 2007; Cannon, 2011; Alaya *et al.*, 2016); and determine scaling relationships between temperature and extreme precipitation (Wasko and Sharma, 2014), among other applications.

Quantile regression equations can be linear or nonlinear. In most variants, including the original linear model (Koenker and Bassett Jr., 1978), conditional quantiles for specified quantile probabilities are estimated separately by different regression equations; together, these different equations can be used to build up a piecewise estimate of the conditional response distribution. However, given finite samples, this flexibility can lead to “quantile crossing” where, for some values of the covariates, quantile regression predictions do not increase with the specified quantile probability τ . For instance, the $\tau_1 = 0.1$ -quantile (10th-percentile) estimate may be greater in magnitude than the $\tau_2 = 0.2$ -quantile (20th-percentile) estimate, which violates the property that the conditional quantile function be strictly monotonic. As Ouali *et al.* (2016) state, “crossing quantile regression is a serious modeling problem that may lead to an invalid response distribution”.

Three main approaches have been used to solve the quantile crossing problem: post-processing, stepwise estimation, and simultaneous estimation. In post-processing, non-crossing quantiles are enforced following model estimation by rearranging predictions so that they increase with increasing τ (Chernozhukov *et al.*, 2010). In stepwise estimation, regression equations are constructed

59 iteratively, with constraints added so that each subsequent quantile regression function does not
60 cross the one estimated previously (*Liu and Wu, 2009; Muggeo et al., 2013*). Finally, in simultane-
61 ous estimation, quantile regression equations for all desired values of τ are estimated at the same
62 time, with additional constraints added to parameter optimization to ensure non-crossing (*Takeuchi*
63 *et al., 2006; Bondell et al., 2010; Liu and Wu, 2011; Bang et al., 2016*). Unlike sequential esti-
64 mation, simultaneous estimation is attractive because it does not depend on the order in which
65 quantiles are estimated. Furthermore, fitting for multiple values of τ simultaneously allows one
66 to “borrow strength” across regression quantiles and improve overall model performance (*Bang*
67 *et al., 2016*). This property is especially useful for nonlinear quantile regression models, which
68 are more prone to overfitting and quantile crossing in the face of small to moderate sample sizes
69 (*Muggeo et al., 2013*).

70 When confronted with the flexibility of a nonlinear model, imposing extra constraints along-
71 side non-crossing can be useful. Growth curves, for example, should increase monotonically with
72 the age of the organism, which led *Muggeo et al. (2013)* to introduce a monotonicity constraint
73 in addition to the non-crossing constraint. Similarly, *Roth et al. (2015)* applied nonlinear mono-
74 tone quantile regression to describe non-decreasing trends in rainfall extremes. *Takeuchi et al.*
75 *(2006)* developed a nonparametric, kernelized version of quantile regression with similarities to
76 support vector machines; both non-crossing and monotonicity constraints are considered, with di-
77 rections on the incorporation of other constraints, such as positivity and additivity constraints, also
78 provided. However, standard implementations of the kernel quantile regression model (e.g., *Karat-*
79 *zoglou et al., 2004; Hofmeister, 2017*) are computationally costly, with complexity that is cubic in
80 the number of samples, and do not explicitly implement the proposed constraints.

81 As an alternative, this study introduces an efficient, flexible nonlinear quantile regression
82 model, the monotone composite quantile regression neural network (MCQRNN), that: (1) simulta-
83 neously estimates multiple non-crossing quantile functions; (2) allows for optional monotonicity,
84 positivity/non-negativity, and additivity constraints, as well as fine-grained control on the degree
85 of non-additivity; and (3) can be modified to estimate standard least-squares regression and non-

86 crossing expectile regression functions. Development of the MCQRNN model combines elements
87 of the standard QRNN model by *White (1992)*, *Taylor (2000)* and *Cannon (2011)*; the monotone
88 multi-layer perceptron (MMLP) by *Zhang and Zhang (1999)*, *Lang (2005)*, and *Minin et al. (2010)*;
89 the composite QRNN (CQRNN) and expectile regression neural network by *Xu et al. (2017)* and
90 *Jiang et al. (2017)* respectively; and the generalized additive neural network by *Potts (1999)*.

91 The MCQRNN model is developed in Section 2, starting from the MMLP model, leading to
92 the MQRNN model, and then finally to the full MCQRNN. Approaches to enforce monotonicity,
93 positivity/non-negativity, and generalized additive model constraints, as well as to estimate un-
94 certainty in the conditional τ -quantile functions, are also provided. In Section 3, the MCQRNN
95 model is compared via Monte Carlo simulation to standard MLP, QRNN, and CQRNN models
96 using combinations of three functions and error distributions from *Xu et al. (2017)*. In Section 4,
97 the MCQRNN model is applied to real-world climate data by estimating IDF curves at ungauged
98 locations in Canada based on annual maximum rainfall series at neighbouring gauging stations.
99 IDF curves, which are used in the design of civil infrastructure such as culverts, storm sewers,
100 dams, and bridges, summarize the relationship between the intensity and occurrence frequency
101 of extreme rainfall over averaging durations ranging from minutes to a day (*Canadian Standards*
102 *Association, 2012*). The intensity of extreme rainfall, a non-negative quantity, should increase
103 monotonically as the annual probability of occurrence decreases (e.g., from $1 - \tau = 0.5$ to 0.01
104 or, equivalently, a 2-yr to 100-yr return period) and as the storm duration decreases (e.g., from
105 24-hr to 5-min). Monotonicity and positivity/non-negativity constraints are thus key features of
106 an IDF curve. MCQRNN IDF curve estimates are compared with those obtained by fitting sepa-
107 rate QRNN models for each return period and duration, as done previously by *Ouali and Cannon*
108 (2017). Finally, Section 5 provides closing remarks and suggestions for future research.

2 Modelling framework

2.1 Monotone multi-layer perceptron (MMLP)

The monotone composite quantile regression neural network (MCQRNN) model starts with the multi-layer perceptron (MLP) neural network with partial monotonicity constraints (Zhang and Zhang, 1999) as its basis. For a data point with index t , the prediction $\hat{y}(t)$ from a monotone MLP (MMLP) is obtained as follows. First, the V covariates, each assumed to be standardized to zero mean and unit standard deviation, are separated into two groups: $x_{m \in M}(t)$ and $x_{i \in I}(t)$ with combined indices $\{M \cup I \mid 1, \dots, V, V = (\#M + \#I)\}$, where M is the set of indices for covariates with a monotone increasing relationship with the prediction, I is the corresponding set of indices for covariates without monotonicity constraints, and $\#$ denotes the number of set elements. Covariates are transformed into $j = 1, \dots, J$ hidden layer outputs

$$h_j(t) = f \left(\sum_{m \in M} x_m(t) \exp(W_{mj}^{(h)}) + \sum_{i \in I} x_i(t) W_{ij}^{(h)} + b_j^{(h)} \right) \quad (1)$$

where $\mathbf{W}^{(h)}$ is a $V \times J$ parameter matrix, $\mathbf{b}^{(h)}$ is a vector of J intercept parameters, and f is a smooth non-decreasing function, usually taken to be the hyperbolic tangent function. Finally, the model prediction is given as a weighted combination of the J hidden layer outputs

$$\hat{y}(t) = g \left(\sum_{j=1}^J h_j(t) \exp(w_j) + b \right) \quad (2)$$

where \mathbf{w} is a vector of J parameters, b is an intercept term, and g is a smooth non-decreasing inverse-link function.

Because both f and g are non-decreasing, partial monotonicity constraints (i.e., $\frac{\partial \hat{y}}{\partial x_m} \geq 0$ everywhere) can be imposed by ensuring that all parameters leading from each monotone-constrained covariate x_m are positive (Zhang and Zhang, 1999), in this case by applying the exponential function to the corresponding elements of $\mathbf{W}^{(h)}$ and all elements of \mathbf{w} . Decreasing relationships can be imposed by multiplying covariates by -1 . Also, extra hidden layers of positive parameters can

130 be added to the model. As pointed out by *Lang (2005)* and *Minin et al. (2010)*, an additional hid-
 131 den layer is required for the MMLP to maintain its universal function approximation capabilities.
 132 While multiple hidden layers are implemented by *Cannon (2017)*, for sake of simplicity, this study
 133 only considers the single hidden layer architecture of *Zhang and Zhang (1999)*. In practice, simple
 134 functional relationships can still be represented by a single hidden layer model.

135 If M is the empty set and the positivity constraint on the \mathbf{w} parameters is removed, this leads
 136 to the standard MLP model. If f and g are the identity function, the MMLP reduces to a linear
 137 model. If f is nonlinear, then the model can represent nonlinear relationships, including those
 138 involving interactions between covariates; the number of hidden layer outputs J further controls
 139 the potential complexity of the MLP mapping. All models in this study set f to be the hyperbolic
 140 tangent function.

141 2.2 Monotone quantile regression neural network (MQRNN)

142 Adjustable parameters $(\mathbf{W}^{(h)}, \mathbf{b}^{(h)}, \mathbf{w}, b)$ in the MMLP are set by minimizing the least squares (LS)
 143 error function

$$E_{\text{LS}} = \frac{1}{N} \sum_{t=1}^N (y(t) - \hat{y}(t))^2 \quad (3)$$

144 over a training dataset with N data points $\{(\mathbf{x}(t), y(t)) \mid t = 1, \dots, N\}$, where $y(t)$ is the target value
 145 of the response variable. While LS regression is most common, different error functions are appro-
 146 priate for different prediction tasks. Minimizing the LS error function is equivalent to maximum
 147 likelihood estimation for the conditional mean assuming a Gaussian error distribution with con-
 148 stant variance (i.e., a traditional regression task), while minimizing the least absolute error (LAE)
 149 function

$$E_{\text{LAE}} = \frac{1}{N} \sum_{t=1}^N |y(t) - \hat{y}(t)| \quad (4)$$

150 leads to a regression estimate for the conditional median (i.e., the $\tau = 0.5$ -quantile) (*Koenker and*

151 *Bassett Jr., 1978*).

152 The fundamental quantity of interest here is not just the median, but rather the magnitude of
153 the conditional quantile associated with the quantile probability τ ($0 < \tau < 1$). In this context,
154 minimizing the asymmetric absolute value error function

$$E_\tau = \frac{1}{N} \sum_{t=1}^N \rho_\tau(y(t) - \hat{y}(t)) \quad (5)$$

155 where

$$\rho_\tau(\varepsilon) = \begin{cases} \tau \varepsilon & \varepsilon \geq 0 \\ (\tau - 1) \varepsilon & \varepsilon < 0 \end{cases} \quad (6)$$

156 leads to estimates of the conditional τ -quantile function (*Koenker and Bassett Jr., 1978*). When
157 $\tau = 0.5$, equation 5 is, up to a constant scaling factor, the same as the LAE function (equation 4) that
158 yields the conditional median; for $\tau \neq 0.5$, the asymmetric absolute value function gives different
159 weight to positive/negative deviations. For example, fitting a model with $\tau = 0.95$ provides an
160 estimate for the conditional 95th-percentile, i.e., a covariate-dependent probability of exceedance
161 of 5%.

162 Combining the MMLP architecture from Section 2.1 with the quantile regression error function
163 results in the MQRNN model. Relaxing the monotonicity constraints gives the standard QRNN
164 model (*Cannon, 2011*). Parameters can be estimated by a gradient-based nonlinear optimization
165 algorithm, with calculation of the gradient using backpropagation; given the simple relationship
166 between equations 4 and 5, the analytical expression for the gradient of the quantile regression
167 error function follows from that of the LAE function (*Hanson and Burr, 1988*). In this case,
168 the derivative is undefined at the origin, which means that a smooth approximation is instead
169 substituted for the exact quantile regression error function. Following *Chen (2007)* and *Cannon*
170 (*2011*), a Huber-norm version of equation 6 replaces $\rho_\tau(\varepsilon)$ in the quantile regression error function.
171 This approximation, denoted by (A), is given by

$$\rho_{\tau}^{(A)}(\varepsilon) = \begin{cases} \tau \varphi(\varepsilon) & \varepsilon \geq 0 \\ (\tau - 1) \varphi(\varepsilon) & \varepsilon < 0 \end{cases} \quad (7)$$

172 where the Huber function

$$\varphi(\varepsilon) = \begin{cases} \frac{\varepsilon^2}{2\alpha} & 0 \leq |\varepsilon| \leq \alpha \\ |\varepsilon| - \frac{\alpha}{2} & |\varepsilon| > \alpha \end{cases} \quad (8)$$

173 is a hybrid of the absolute value and squared error functions (*Huber, 1964*).

174 The Huber function transitions smoothly from the squared error, which is applied around the
 175 origin ($\pm\alpha$) to ensure differentiability, and the absolute error. As $\alpha \rightarrow 0$, the approximate er-
 176 ror function converges to the exact quantile regression error function. It should be noted that a
 177 slightly different approximation is used by *Muggeo et al. (2012)*. Based on experimental results
 178 (not shown), both approximations ultimately provide models that are indistinguishable. However,
 179 the Huber function approximation is used here for its added ability to emulate the LS cost func-
 180 tion. For sufficiently large α , all model deviations are squared and the approximate error function
 181 instead becomes an asymmetric version of the LS error function (equation 3). For $\tau = 0.5$ and
 182 large α , the error function is symmetric and is, up to a constant scaling factor, equal to the LS error
 183 function. For $\tau \neq 0.5$, the asymmetric LS error function results in an estimate of the conditional
 184 expectile function (*Newey and Powell, 1987; Yao and Tong, 1996; Waltrup et al., 2015*). Hence,
 185 depending on values of α and τ , minimizing the approximate quantile regression error function can
 186 provide regression estimates for the conditional mean ($\alpha \gg 0, \tau = 0.5$), median ($\alpha \rightarrow 0, \tau = 0.5$),
 187 quantiles ($\alpha \rightarrow 0, 0 < \tau < 1$), and expectiles ($\alpha \gg 0, 0 < \tau < 1$) (*Jiang et al., 2017*). Unless noted
 188 otherwise, all subsequent references to $\rho_{\tau}^{(A)}$ and $E_{\tau}^{(A)}$ will refer to the conditional quantile form of
 189 the Huber function approximation.

190 Unlike linear regression, where the total number of model parameters is limited by the number
 191 of covariates V , the complexity of the MQRNN model also depends on the number of hidden layer
 192 outputs J . Model complexity, and hence J , should be set such that the model can generalize to

193 new data, which, in practice, usually means avoiding overfitting to noise in the training dataset.
 194 Additionally, regularization terms that penalize the magnitude of the parameters, hence limiting
 195 the nonlinear modelling capability of the model, can be added to the error function

$$\tilde{E}_\tau^{(A)} = E_\tau^{(A)} + \lambda^{(h)} \frac{1}{VJ} \sum_{i=1}^V \sum_{j=1}^J \left(W_{ij}^{(h)} \right)^2 + \lambda \frac{1}{J} \sum_{j=1}^J (w_j)^2 \quad (9)$$

196 where $\lambda^{(h)} \geq 0$ and $\lambda \geq 0$ are hyperparameters that control the size of the penalty applied to the
 197 elements of $\mathbf{W}^{(h)}$ and \mathbf{w} respectively. Values of J and, optionally, the $\lambda^{(h)}$ and λ hyperparame-
 198 ters are typically set by minimizing out-of-sample generalization error, for example as estimated
 199 via cross-validation or modified versions of an information criterion like the Akaike information
 200 criterion (QAIC) (Koenker and Schorfheide, 1994; Doksum and Koo, 2000)

$$\text{QAIC} = -2 \log(E_\tau) + 2p \quad (10)$$

202 where p is an estimate of the effective number of model parameters.

203 **2.3 Monotone composite quantile regression neural network (MCQRNN)**

204 The MQRNN model in Section 2.2 is specified for a single τ -quantile; no efforts are made to avoid
 205 quantile crossing for multiple estimates. To date, the simultaneous estimation of multiple non-
 206 crossing τ -quantiles has not been considered for QRNN models. However, simultaneous estimates
 207 for multiple values of τ are used in the composite QRNN (CQRNN) model proposed by Xu *et al.*
 208 (2017). CQRNN shares the same goal as the linear composite quantile regression (CQR) model
 209 (Zou and Yuan, 2008), namely to borrow strength across multiple regression quantiles to improve
 210 the estimate of the true, unknown relationship between the covariates and the response. This
 211 is especially valuable in situations where the error follows a heavy-tailed distribution. In CQR,
 212 the regression coefficients are shared across the different quantile regression models; similarly, in
 213 CQRNN, the $\mathbf{W}^{(h)}$, $\mathbf{b}^{(h)}$, \mathbf{w} , b parameters are shared across the different QRNN models. Hence,
 214 the models are not explicitly trying to describe the full conditional response distribution, but rather
 215 a single function that best describes the true covariate-response relationship.

216 Structurally, the CQRNN model is the same as the QRNN model. The only difference is the
 217 quantile regression error function, which is now summed over K (usually equally spaced) values
 218 of τ

$$E_{C\tau}^{(A)} = \frac{1}{KN} \sum_{k=1}^K \sum_{t=1}^N \rho_{\tau_k}^{(A)}(y(t) - \hat{y}_{\tau_k}(t)) \quad (11)$$

219 where, for example, $\tau_k = \frac{k}{K+1}$ for $k = 1, 2, \dots, K$. Penalty terms can be added as in equation 9.

220 The MCQRNN model combines the MMLP/MQRNN model architecture with the composite
 221 quantile regression error function to simultaneously estimate non-crossing regression quantiles. To
 222 show how this is achieved, consider an $N \times \#I$ matrix of covariates \mathbf{X} , a corresponding response
 223 vector \mathbf{y} of length N , and the goal of estimating non-crossing quantile functions for $\tau_1 < \tau_2 <$
 224 $\dots < \tau_K$. First, create a new $\#M = 1$ monotone covariate vector $\mathbf{x}_m^{(S)}$ of length $S = KN$, where (S)
 225 denotes stacked data, by repeating each of the K specified τ values N times and stacking. Next,
 226 stack K copies of \mathbf{X} and concatenate with $\mathbf{x}_m^{(S)}$ to form a stacked covariate matrix $\mathbf{X}^{(S)}$ of dimension
 227 $S \times (1 + \#I)$. Finally stack K copies of \mathbf{y} to form $\mathbf{y}^{(S)}$. Taken together, this gives the stacked dataset

$$\mathbf{X}^{(S)} = \begin{bmatrix} \tau_1 & x_1(1) & \cdots & x_{\#I}(1) \\ \vdots & \vdots & \ddots & \vdots \\ \tau_1 & x_1(N) & \cdots & x_{\#I}(N) \\ \tau_2 & x_1(1) & \cdots & x_{\#I}(1) \\ \vdots & \vdots & \ddots & \vdots \\ \tau_2 & x_1(N) & \cdots & x_{\#I}(N) \\ \vdots & \vdots & \ddots & \vdots \\ \tau_K & x_1(1) & \cdots & x_{\#I}(1) \\ \vdots & \vdots & \ddots & \vdots \\ \tau_K & x_1(N) & \cdots & x_{\#I}(N) \end{bmatrix}, \mathbf{y}^{(S)} = \begin{bmatrix} y(1) \\ \vdots \\ y(N) \\ y(1) \\ \vdots \\ y(N) \\ \vdots \\ y(1) \\ \vdots \\ y(N) \end{bmatrix} \quad (12)$$

228 which is used to fit the MQRNN model. By treating the τ values as a monotone covariate, predic-
 229 tions $\hat{y}^{(S)}$ from equations 1 and 2 for fixed values of the non-monotone covariates are guaranteed to

230 increase with τ . Non-crossing is imposed by construction. Defining $\tau(s) = x_1^{(S)}(s)$, the composite
 231 quantile regression error function for the stacked data can be written as

$$E_{C\tau}^{(A,S)} = \sum_{s=1}^S \omega_{\tau(s)} \rho_{\tau(s)}^{(A)} \left(y^{(S)}(s) - \hat{y}_{\tau(s)}^{(S)}(s) \right) \quad (13)$$

232 where $\omega_{\tau(s)}$ are weights that can be used to allow regression quantiles for each τ_k to contribute
 233 different amounts to the total error (*Jiang et al.*, 2012; *Sun et al.*, 2013); constant weights $\omega_{\tau(s)} =$
 234 $1/S$ lead to the standard composite quantile regression error function. Minimization of equation
 235 13 results in the fitted MCQRNN model. (Note: non-crossing expectile regression models can
 236 be obtained by adjusting $\alpha \gg 0$ in $\rho_{\tau}^{(A)}$.) Following model estimation, conditional τ -quantile
 237 functions can be predicted for any value of $\tau_1 \leq \tau \leq \tau_K$ by entering the desired value of τ into the
 238 monotone covariate.

239 To illustrate, Figure 1 shows results from a MCQRNN model ($J = 4$, $\lambda^{(h)} = 0.00001$, $\lambda = 0$,
 240 $K = 9$, $\tau = 0.1, 0.2, \dots, 0.9$) fit to 500 samples of synthetic data for the two functions from *Bondell*
 241 *et al.* (2010)

$$y_1 = 0.5 + 2x + \sin(2\pi x - 0.5) + \varepsilon \quad (14)$$

242 and

$$y_2 = 3x + [0.5 + 2x + \sin(2\pi x - 0.5)] \varepsilon \quad (15)$$

243 where x is drawn from the standard uniform distribution $x \sim U(0, 1)$ and ε from the standard
 244 normal distribution $\varepsilon \sim N(0, 1)$. All τ are weighted equally in equation 13 (i.e., values of $\omega_{\tau(s)}$
 245 are constant). Results are compared with those from separate QRNN models ($J = 4$ and $\lambda^{(h)} =$
 246 0.00001) for each τ -quantile. Quantile curves cross for QRNN, especially at the boundaries of
 247 the training data, whereas the MCQRNN model is able to simultaneously estimate multiple non-
 248 crossing quantile functions that correspond more closely to the true conditional quantile functions.
 249 While quantile crossing in QRNN models can be minimized by selecting and applying a suitable

250 weight penalty (*Cannon, 2011*), non-crossing cannot be guaranteed, whereas MCQRNN models
251 impose this constraint by construction.

252 [Figure 1 about here.]

253 **2.4 Additional constraints and uncertainty estimates**

254 As mentioned above, constraints in addition to non-crossing of quantile functions may be useful
255 for some MCQRNN modelling tasks. Partial monotonicity constraints for specified covariates can
256 be imposed as described in Section 2.1; positivity or non-negativity constraints can be added by
257 setting g in equation 2 to the exponential or smooth ramp function (*Cannon, 2011*), respectively;
258 and covariate interactions can be restricted by the approach described in Appendix 1.

259 A form of the parametric bootstrap can be used to estimate uncertainty in the conditional τ -
260 quantile functions. While the MCQRNN model is explicitly optimized for K specified values
261 of τ , the use of the quantile probability as a monotone covariate means that conditional τ -quantile
262 functions can be interpolated for any value of $\tau_1 \leq \tau \leq \tau_K$. Proper distribution, probability density,
263 and quantile functions can then be constructed by assuming a parametric form for the tails of the
264 distribution (*Quiñonero Candela et al., 2006; Cannon, 2011*). The parametric bootstrap proceeds
265 by drawing random samples from the resulting conditional distribution, refitting the MCQRNN
266 model, making estimates of the conditional τ -quantiles, and repeating many times. Confidence
267 intervals are estimated from the bootstrapped conditional τ -quantiles.

268 For illustration, examples of MCQRNN model outputs with positivity and monotonicity con-
269 straints, as well as confidence intervals obtained by the parametric bootstrap, are shown in Figure
270 2 for the two *Bondell et al. (2010)* functions.

271 [Figure 2 about here.]

272 3 Monte Carlo simulation

273 Given the close relationship between the MCQRNN and CQRNN models, performance is first
 274 assessed via Monte Carlo simulation using the experimental setup adopted by *Xu et al. (2017)*
 275 to assess CQRNN. The MCQRNN model is compared with standard MLP, QRNN, and CQRNN
 276 models on datasets generated for three example functions:

$$(example\ 1) \quad y = \sin(2x_1) + 2 \exp(-16x_2^2) + 0.5\varepsilon \quad (16)$$

277 where $x_1 \sim N(0, 1)$ and $x_2 \sim N(0, 1)$;

$$(example\ 2) \quad y = (1 - x + 2x^2) \exp(-0.5x^2) + \frac{(1 + 0.2x)}{5} \varepsilon \quad (17)$$

278 where $x \sim U(-4, 4)$; and

$$(example\ 3) \quad y = \frac{40 \exp\{8[(x_1 - 0.5)^2 + (x_2 - 0.5)^2]\}}{\exp\{8[(x_1 - 0.2)^2 + (x_2 - 0.7)^2]\} + \exp\{8[(x_1 - 0.7)^2 + (x_2 - 0.7)^2]\}} + \varepsilon \quad (18)$$

279 where $x_1 \sim U(0, 1)$ and $x_2 \sim U(0, 1)$. For each of the three functions, random errors are generated
 280 from three different distributions: the normal distribution $\varepsilon \sim N(0, 0.25)$, Student's t distribution
 281 with three degrees of freedom $\varepsilon \sim t(3)$, and the chi-squared distribution with three degrees of
 282 freedom $\varepsilon \sim \chi^2(3)$. Monte Carlo simulations are performed for the nine resulting datasets.

283 For each example and error distribution, 400 samples are generated and split randomly into
 284 200 training and 200 testing samples. Results for QRNN, MLP, CQRNN, and MCQRNN models
 285 are compared by fitting to the training samples and evaluating on the testing samples. Simulations
 286 are repeated 1000 times. Following *Xu et al. (2017)*, the number of hidden layer outputs in all
 287 models is set to $J = 4$ for example 1 and $J = 5$ for examples 2 and 3; for sake of simplicity, no
 288 penalty terms are added when fitting any of the models. The goal is to estimate the true functional
 289 relationship specified by equations 16 to 18. The QRNN model is fit for $\tau = 0.5$, whereas CQRNN

290 and MCQRNN models use $K = 19$ equally spaced values of τ . In the case of MCQRNN, evalua-
291 tions are based on an estimate of the conditional mean function obtained by taking the mean over
292 predictions for the $K = 19$ τ -quantiles. Performance is measured by the root mean squared error
293 (RMSE) between model predictions for the test samples and the actual values of y . Results are
294 shown in Table 1 and Figure 3.

295 [Table 1 about here.]

296 [Figure 3 about here.]

297 As expected, the MLP model, which is fit using the LS error function and hence is optimal for
298 normally distributed errors with constant variance, tends to perform best for the three examples
299 when $\varepsilon \sim N(0, 0.25)$. MCQRNN performs similarly well for normally distributed errors – in all
300 cases, median values of RMSE are within 1% of the MLP model (Table 1) – whereas QRNN and
301 CQRNN, which share the same median RMSE values, lag slightly behind. For the two non-normal
302 error distributions, $\varepsilon \sim t(3)$ and $\varepsilon \sim \chi^2(3)$, MCQRNN clearly outperforms the other models; it
303 has the lowest median RMSE in 5 out of the 6 cases and is the top performing model in terms of
304 RMSE rank in all six cases (Figure 3). MLP tends to perform the worst for $\varepsilon \sim t(3)$, whereas MLP,
305 QRNN, and CQRNN each perform worst for different examples when $\varepsilon \sim \chi^2(3)$.

306 Overall, the MCQRNN model performs well on the synthetic data from *Xu et al. (2017)*. In the
307 next section, the modelling framework is applied to real-world climate data. As a proof of concept,
308 rainfall IDF curves are estimated by MCQRNN at ungauged locations in Canada and, following
309 *Ouali and Cannon (2017)*, results are compared against those obtained from QRNN models.

310 **4 Rainfall IDF curves**

311 **4.1 Data**

312 IDF curves provided by Environment and Climate Change Canada (ECCC) summarize the rela-
313 tionship between annual maximum rainfall intensity for different frequencies of occurrence (2-,

314 5-, 10-, 25-, 50-, and 100-yr return periods, i.e., $\tau = 0.5, 0.8, 0.9, 0.96, 0.98, 0.99$ -quantiles) and
315 durations ($D = 5$ -, 10-, 15-, 30-, 60-min, 2-, 6-, 12-, and 24-hr) at locations with long records of
316 short-duration rainfall rate observations. Example IDF curves for Victoria Intl A, a station on the
317 southwest coast of British Columbia, Canada, are shown in Figure 4. Annual maximum rainfall
318 rate data for durations from 5-min to 24-hr are obtained from the Engineering Climate Datasets
319 of ECCC (*Environment and Climate Change Canada*, 2014). The rainfall rate dataset is based on
320 tipping bucket rain gauge observations at 565 stations across Canada (Figure 5). Record lengths
321 range from 10-yr to 81-yr, with a median length of 25-yr. Information on the observing program,
322 quality control, and quality assurance methods is provided in detail by *Shephard et al.* (2014).

323 [Figure 4 about here.]

324 [Figure 5 about here.]

325 Official ECCC IDF curves are constructed by first fitting the parametric Gumbel distribution
326 to annual maximum rainfall rate series at each site for each duration. Naturally, this approach
327 cannot provide quantile estimates for locations where short-duration rainfall observations are not
328 observed. Parametric extreme value distributions, fit in conjunction with regionalization or regional
329 regression models, have been used to estimate IDF curves at ungauged locations in Canada by
330 *Alila* (1999, 2000), *Kuo et al.* (2012), and *Mailhot et al.* (2013). As a non-parametric alternative
331 to standard parametric approaches, *Ouali and Cannon* (2017) recently evaluated regional QRNN
332 models for IDF curves at ungauged locations. While results suggest that the QRNN model can
333 outperform standard parametric methods, further improvements are still possible. In particular,
334 *Ouali and Cannon* (2017) fit separate QRNN models for each τ -quantile and duration, which
335 means that quantile crossing is possible; further, rainfall intensities may not increase as storm
336 duration decreases. Instead, use of the MCQRNN is proposed to ensure non-crossing quantiles
337 and a monotone decreasing relationship with increasing storm duration.

338 In addition to the short-duration rainfall rate data, which serves as the response variable in
339 the MCQRNN model, covariates are required to estimate rainfall intensities at ungauged sites

340 based on information available at gauged sites. Five variables, including latitude, longitude, and
341 elevation, as well as climatological winter and summer mean precipitation (*McKenney et al.*, 2011),
342 are used here as covariates. Estimation at ungauged sites typically relies on pooling gauged data
343 from a homogeneous region around the site of interest, whether in geographic space or some
344 derived hydroclimatological space (*Ouarda et al.*, 2001), and then fitting a regression model linking
345 the spatial covariates with the short-duration rainfall rate response. As the focus of this study is
346 on methods for conditional quantile estimation, and not the delineation of homogeneous regions,
347 regionalizations here are based on a simple geographic region-of-influence in which data from the
348 80 nearest gauged sites are pooled together. Following *Aziz et al.* (2014), this emphasizes the use
349 of data from a large number of sites rather than the most homogeneous sites; it is then up to the
350 regression model to infer relevant covariate-response relationships from within this larger pool of
351 data. In areas with low station density, however, it is questionable whether any statistical regional
352 frequency analysis technique can be used to reliably estimate rainfall extremes. Performance in
353 sparsely monitored regions will be explored as part of the subsequent model evaluation.

354 **4.2 Cross-validation results**

355 Regional MCQRNN and QRNN models for IDF curves are evaluated via leave-one-out cross-
356 validation. Each of the 565 observing sites is treated, in turn, as being “ungauged”; data from
357 nearest 80 sites are used to fit the models, model predictions are made at the left-out site, and model
358 performance statistics are calculated based on the left-out data. Following *Ouali and Cannon*
359 (2017), 54 separate QRNN models are fit for each site, one for each combination of the 9 durations
360 ($D = 5\text{-min to } 24\text{-hr}$) and 6 τ -quantiles ($\tau = 0.5 \text{ to } 0.99$) reported in ECCC IDF curves. Each
361 MCQRNN model combines data for all 9 values of D and fits non-crossing quantile curves for the
362 6 τ -quantiles simultaneously.

363 Non-negativity constraints are imposed in both QRNN and MCQRNN models by setting g
364 to the smooth ramp function (*Cannon*, 2011). Monotonicity constraints – increasing with τ and
365 decreasing with D – are imposed in the MCQRNN model by adopting the MMLP architecture

366 with additional monotone covariates [τ and $-\log(D)$]. The optimum level of complexity for each
 367 kind of model is selected based on values of QAIC, here based on the composite QR error function
 368 (e.g., *Xu et al.*, 2017), averaged over all sites, from candidates with $J = 1, 2, \dots, 5$ (*Koenker and*
 369 *Schorfheide*, 1994; *Doksum and Koo*, 2000; *Xu et al.*, 2017). The number of hidden nodes J is
 370 fixed to the same value for all sites in the study domain. QAIC is minimized for QRNN models
 371 with $J = 1$ and MCQRNN models with $J = 3$.

372 [Table 2 about here.]

373 Cross-validation results comparing the MCQRNN ($J = 3$) and QRNN ($J = 1$) models are
 374 reported in terms of relative differences in leave-one-out estimates of the quantile regression error
 375 function

$$\text{RD}_\tau = 100 \left(\frac{E_\tau^{(\text{MCQRNN})} - E_\tau^{(\text{QRNN})}}{E_\tau^{(\text{QRNN})}} \right) \quad (19)$$

376 summed over all stations for each return period and duration. Values are shown in Table 2a.
 377 Because the underlying model architecture is, aside from different values of J and inclusion of
 378 monotonicity constraints, fundamentally the same for the QRNN and MCQRNN models, it is
 379 not surprising that the two perform similarly well. MCQRNN and QRNN errors fall within 5%
 380 of one another for nearly all combinations of return period and duration, although MCQRNN
 381 tends to perform slightly better for short durations ($D = 5\text{-min to } 2\text{-hr}$) and QRNN for longer
 382 durations ($D = 6\text{-hr to } 24\text{-hr}$). Poorer performance of the MCQRNN model in these cases is partly
 383 attributable to the smaller rainfall intensities that are associated with long duration storms being
 384 weighted less in the CQR cost function (equation 13) than the larger intensities that accompany
 385 short duration storms. This can be remedied by setting $\omega_{\tau(s)} \propto \log(D)$ in equation 13. Results
 386 for the MCQRNN model with weighting are shown in Table 2b. Weighting improves performance
 387 for longer durations, while having minimal impact on shorter durations. Further results will be
 388 reported for the weighted MCQRNN model.

389 Despite the similar levels of quantile error, the additional MCQRNN monotonicity constraints

390 on τ and D leads to IDF curves that are guaranteed to increase as occurrence frequency and storm
391 duration decrease, properties that need not be present for QRNN predictions. This is evident for
392 Victoria Intl A (Figure 6), where quantile crossing and non-monotone increasing behaviour with
393 decreasing storm duration is noted for the 100-yr QRNN model predictions (cf. Figure 4).

394 [Figure 6 about here.]

395 Each of the QRNN ($J = 1$) models for the 54 combinations of τ and D contain $J(\#I + 1) +$
396 $J + 1 = 1(5 + 1) + 1 + 1 = 8$ parameters or 432 parameters in total. Because it borrows strength
397 over τ and D , the MCQRNN ($J = 3$) model requires just $J(\#I + \#M + 1) + J + 1 = 3(5 + 2 + 1) +$
398 $3 + 1 = 28$ shared parameters for the same task. Given that the two models show similar levels
399 of performance, parameters in the separate QRNN equations must be largely redundant. If model
400 complexity is increased, for example to $J = 5$, the total number of estimated parameters is 1,944 for
401 QRNN (36 for each combination of τ and D) versus 46 for MCQRNN. By way of comparison, the
402 at-site (rather than ungauged) ECCC IDF curves require estimation of 30 parameters (18 Gumbel
403 distribution and 12 interpolation equation parameters).

404 [Figure 7 about here.]

405 Do the non-crossing/monotonicity constraints and ability to borrow strength provide a guard
406 against overfitting if MCQRNN model complexity is misspecified? Figure 7 shows relative dif-
407 ferences RD_τ in cross-validated quantile regression error for MCQRNN and QRNN models with
408 $J = 1, 2, \dots, 5$; in both cases, the optimal QRNN ($J = 1$) model serves as the reference. Consis-
409 tent with results from QAIC model selection, cross-validated QRNN errors increase when $J > 1$.
410 When using more than the recommended number of hidden nodes, the QRNN performs poorly,
411 especially for long return period estimates. However, for MCQRNN, in the absence of underfitting
412 (i.e., $J = 1$), there is little penalty for specifying an overly complex model. Performance of the
413 optimal MCQRNN ($J = 3$) model recommended by QAIC model selection is nearly identical to
414 that of the misspecified $J = 5$ model. The non-crossing constraint provides strong regularization
415 and resistance to overfitting.

416

[Table 3 about here.]

417 Results reported so far have compared leave-one-out cross-validation performance of the MC-
 418 QRNN and QRNN models. This does not provide any indication of how well the ungauged pre-
 419 dictions compare with those estimated by the at-site ECCC IDF curve procedure, i.e., by fitting
 420 the Gumbel distribution and log linear interpolating equations to observed annual maxima at each
 421 station. Following *Ouali and Cannon (2017)*, the ability of the MCQRNN to replicate the at-site
 422 ECCC IDF curves is measured by the quantile regression error ratio

$$R_{\tau} = \frac{E_{\tau}'^{(\text{ECCC})}}{E_{\tau}^{(\text{MCQRNN})}} \quad (20)$$

423 where $E_{\tau}'^{(\text{ECCC})}$ is the in-sample, at-site quantile regression error of the ECCC IDF curve interpo-
 424 lating equations. A value of 1 means that ungauged MCQRNN predictions reach the same level
 425 of error as the at-site ECCC IDF curves. Note: even though the ECCC IDF curves are calculated
 426 from observations at each station, it is possible for R_{τ} to exceed 1 as the annual maximum rainfall
 427 data may deviate from the assumed Gumbel distribution and log linear form of the interpolating
 428 equations. Results are summarized in Table 3. Values exceed 0.75 for all combinations of D and
 429 τ , with values greater than 0.9 noted for return periods from 2-yr to 10-yr for all D .

430

[Figure 8 about here.]

431 As shown in Figure 5, stations are not evenly distributed across Canada; northern latitudes,
 432 in particular, are very sparsely gauged. Does MCQRNN performance depend on station density?
 433 Values of R_{τ} , stratified by the median distance of each ungauged station to its 80 neighbours, are
 434 shown in Figure 8. As expected, errors are nearly equivalent ($R_{\tau} > 0.975$) to the at-site estimates
 435 in areas of high station density (median distances < 100 -km). Modest performance declines are
 436 noted ($R_{\tau} > 0.875$) with increasing median distance up to 500-km, beyond which performance
 437 degrades more substantially, especially for the longest return periods ($R_{\tau=0.99} < 0.8$). The viability
 438 of ungauged estimation should be evaluated carefully in areas of low station density.

5 Conclusion

This study introduces a novel form of quantile regression that can be used to simultaneously estimate multiple non-crossing, nonlinear quantile regression functions. The MCQRNN model architecture, which is based on the standard MLP neural network, allows optional monotonicity, positivity/non-negativity, and generalized additive model constraints to be imposed in a straightforward manner. As an extension, a simple way to control the strength of non-additive relationships is also provided. The Huber function approximation to the QR error function means that standard least-squares regression and non-crossing expectile regression functions can be estimated using the same model architecture.

Given its close relationship to composite QR models, MCQRNN is first evaluated using the Monte Carlo simulation experiments adopted by *Xu et al. (2017)* to demonstrate the CQRNN model. In comparison to MLP, QRNN, and CQRNN models, MCQRNN outperforms the other models for non-normal error distributions and reaches the same level of performance as the optimal MLP model for the normal error distribution. Next, the MCQRNN model is evaluated on real-world climate data by estimating rainfall IDF curves in Canada. Cross-validation results suggest that the MCQRNN effectively borrows strength across different storm durations and return periods, which results in a model that is robust against overfitting. In comparison to standard QRNN, the ability of the MCQRNN model to incorporate monotonicity constraints – rainfall intensity should increase monotonically as the occurrence frequency and storm duration decrease – leads to more realistic estimates of extreme rainfall at ungauged sites. While promising, use of the MCQRNN for IDF curve estimation is presented here as a proof of concept. Other avenues of research include a more principled consideration of regionalization (*Ouarda et al., 2001*), other covariates (*Madsen et al., 2017*), and comparison against a wider range of nonlinear methods (*Ouali et al., 2017*). The MCQRNN model architecture is extremely flexible and many of its features are also not explored in this study. For example, the use of different weights for each τ in the composite QR error function (*Jiang et al., 2012; Sun et al., 2013*), multiple hidden layers, and the ability to estimate non-crossing, nonlinear expectile regression functions (*Jiang et al., 2017*) are left for future research.

466 Finally, code implementing the MCQRNN model is freely available from the Comprehensive
467 R Archive Network as part of the qrn package.

468 **Acknowledgments**

469 The author would like to thank Dae Il Jeong, William Hsieh, and the anonymous reviewers for their
470 constructive feedback. The Comprehensive R Archive Network (CRAN) is acknowledged for host-
471 ing the qrn package <<https://CRAN.R-project.org/package=qrn>> for the R programming
472 language and environment for statistical computing and graphics.

473 **Appendix 1: Additive MLP models and control over non-additivity**

474 As shown by *Potts* (1999), the MLP architecture used by the MCQRNN model can represent
475 generalized additive relationships, i.e., where the model output depends on linear combinations of
476 unknown smooth functions applied to each covariate in turn. Each covariate is associated with its
477 own MLP, separate from those for the other covariates (Figure 9a), which means that interactions
478 between covariates are neglected. The resulting model is easy to interpret, as contributions from
479 covariates can be analyzed in isolation.

480 From Section 2.1 – removing partial monotonicity constraints for sake of simplicity – this is
481 equivalent to representing the hidden layer outputs in the form

$$h_j(t) = f \left(\sum_{i \in I} x_i(t) A_{ij}^{(h)} W_{ij}^{(h)} + b_j^{(h)} \right) \quad (21)$$

482 where $\mathbf{A}^{(h)}$ is an appropriate binary mask. For example, for a model with $\#I = 4$ covariates and $J =$
483 $3(\#I) = 12$ hidden layer outputs, as shown in Figure 9, the mask that enforces additive relationships
484 is given by

$$\mathbf{A}^{(h)} = \begin{bmatrix} 1 & 1 & 1 & 0 & 0 & 0 & 0 & 0 & 0 & 0 & 0 & 0 \\ 0 & 0 & 0 & 1 & 1 & 1 & 0 & 0 & 0 & 0 & 0 & 0 \\ 0 & 0 & 0 & 0 & 0 & 0 & 1 & 1 & 1 & 0 & 0 & 0 \\ 0 & 0 & 0 & 0 & 0 & 0 & 0 & 0 & 0 & 1 & 1 & 1 \end{bmatrix} \quad (22)$$

485 Each of the covariates x_i is passed through a smooth function defined, in this example, by a linear
 486 combination of 3 hidden layer outputs. For a given covariate, the other hidden layer outputs,
 487 and hence covariates, do not contribute to the output because the additive mask multiplies the
 488 corresponding elements of $\mathbf{W}^{(h)}$ by zero (Figure 9b).

489 [Figure 9 about here.]

490 A means of controlling non-additivity in a Gaussian process model was presented by *Plate*
 491 (1999). It was shown that control over interactions in a flexible nonlinear model – allowing for
 492 models that range from being fully additive to those that do not constrain covariate interactions –
 493 can be beneficial for modelling tasks where interpretability and prediction performance are both
 494 important. Similar fine-grained control can be added to models based on the MLP architecture by
 495 removing $\mathbf{A}^{(h)}$ from equation 21 and instead modifying the error function

$$\tilde{E}_\tau^{(A)} = E_\tau^{(A)} + \lambda^{(h)} \frac{1}{VJ} \sum_{i=1}^V \sum_{j=1}^J L_{ij}^{(h)} \left(W_{ij}^{(h)} \right)^2 + \lambda \frac{1}{J} \sum_{j=1}^J (w_j)^2 \quad (23)$$

496 where

$$\mathbf{L}^{(h)} = \begin{bmatrix} 0 & 0 & 0 & 1 & 1 & 1 & 1 & 1 & 1 & 1 & 1 & 1 \\ 1 & 1 & 1 & 0 & 0 & 0 & 1 & 1 & 1 & 1 & 1 & 1 \\ 1 & 1 & 1 & 1 & 1 & 1 & 0 & 0 & 0 & 1 & 1 & 1 \\ 1 & 1 & 1 & 1 & 1 & 1 & 1 & 1 & 1 & 0 & 0 & 0 \end{bmatrix} \quad (24)$$

497 contains the logical negation of elements in the $\mathbf{A}^{(h)}$ matrix that would be applied in a fully-
 498 additive model. In effect, the first penalty term now applies only to elements of $\mathbf{W}^{(h)}$ responsible

499 for controlling interactions between covariates; larger values of $\lambda^{(h)}$ will therefore suppress non-
500 additive relationships.

501 To demonstrate, consider MLP models fit using the modified cost function (equation 23) to
502 synthetic data generated by the function from *Plate* (1999)

$$y = 0.925\phi(x_1, x_2) + 2.248(x_2 + x_3 - 1)^3 + \varepsilon \quad (25)$$

503 where

$$\phi(x_1, x_2) = 1.3356 \left\{ 1.5(1 - x_1) + \exp(2x_1 - 1) \sin \left[3\pi(x_1 - 0.6)^2 \right] + \right. \\ \left. \exp[3(x_2 - 0.5)] \sin \left[4\pi(x_2 - 0.9)^2 \right] \right\} \quad (26)$$

504 Covariate x_1 has a purely additive and nonlinear relationship with the response, while covariates
505 x_2 and x_3 have an interactive, nonlinear relationship. A fourth covariate x_4 , which is irrelevant and
506 does not contribute to the response, is also included. Two datasets are created: training data with
507 300 samples and testing data with 100,000 samples. Each of the four covariates is drawn from a
508 uniform distribution $U(0, 1)$ and $\varepsilon \sim N(0, 0.5)$.

509 Figure 10 shows generalized additive model plots – modified following *Plate* (1999) so that
510 non-additive relationships are indicated by vertical spread in points – for MLP models with $\lambda^{(h)} =$
511 0, 0.2, 1, 100. Values of $\lambda^{(h)} = 0, 0.2$ lead to spurious interactions for x_1 and x_4 , whereas $\lambda^{(h)} =$
512 100 suppresses the true interactions between x_2 and x_3 . $\lambda^{(h)} = 1$ appears to strike the appropriate
513 balance, leading to a MLP model with a nonlinear additive relationship for x_1 , interactions for x_2
514 and x_3 , and no relationship between x_4 and the response. These results are reflected in the measure
515 of interaction strength, training and testing RMSE, and magnitudes of $\mathbf{W}^{(h)}$ elements shown in
516 Figure 11. The MLP with $\lambda^{(h)} = 1$ gives the lowest testing RMSE. This model has strong measured
517 interactions for covariates x_2 and x_3 , which are associated with nonzero elements of $\mathbf{W}^{(h)}$.

518 [Figure 10 about here.]

519 [Figure 11 about here.]

References

- 520
- 521 Alaya, M. B., F. Chebana, and T. Ouarda (2016), Multisite and multivariable statistical downscal-
522 ing using a Gaussian copula quantile regression model, *Climate Dynamics*, 47(5-6), 1383–1397,
523 doi:10.1007/s00382-015-2908-3.
- 524 Alila, Y. (1999), A hierarchical approach for the regionalization of precipitation annual maxima
525 in Canada, *Journal of Geophysical Research: Atmospheres*, 104(D24), 31,645–31,655, doi:
526 10.1029/1999JD900764.
- 527 Alila, Y. (2000), Regional rainfall depth-duration-frequency equations for Canada, *Water Re-*
528 *sources Research*, 36(7), 1767–1778, doi:10.1029/2000WR900046.
- 529 Allamano, P., P. Claps, and F. Laio (2009), Global warming increases flood risk in mountainous
530 areas, *Geophysical Research Letters*, 36(24), doi:10.1029/2009GL041395.
- 531 Aziz, K., A. Rahman, G. Fang, and S. Shrestha (2014), Application of artificial neural networks in
532 regional flood frequency analysis: a case study for Australia, *Stochastic Environmental Research*
533 *and Risk Assessment*, 28(3), 541–554, doi:10.1007/s00477-013-0771-5.
- 534 Bang, S., H. Cho, and M. Jhun (2016), Simultaneous estimation for non-crossing multiple quan-
535 tile regression with right censored data, *Statistics and Computing*, 26(1-2), 131–147, doi:
536 10.1007/s11222-014-9482-0.
- 537 Barbosa, S. M. (2008), Quantile trends in Baltic sea level, *Geophysical Research Letters*, 35(22),
538 doi:10.1029/2008GL035182.
- 539 Bondell, H. D., B. J. Reich, and H. Wang (2010), Noncrossing quantile regression curve estimation,
540 *Biometrika*, 97(4), 825–838, doi:10.1093/biomet/asq048.
- 541 Canadian Standards Association (2012), PLUS 4013 (2nd ed.)—Technical Guide: Development,
542 Interpretation and Use of Rainfall Intensity-Duration-Frequency (IDF) Information: Guideline

543 for Canadian Water Resources Practitioners, *Mississauga, Ontario: Canadian Standards Asso-*
544 *ciation.*

545 Cannon, A. J. (2011), Quantile regression neural networks: Implementation in R and ap-
546 plication to precipitation downscaling, *Computers & Geosciences*, 37(9), 1277–1284, doi:
547 10.1016/j.cageo.2010.07.005.

548 Cannon, A. J. (2017), *qrnn: Quantile Regression Neural Network*, R package version 2.0.1.

549 Cawley, G. C., G. J. Janacek, M. R. Haylock, and S. R. Dorling (2007), Predictive uncertainty in
550 environmental modelling, *Neural Networks*, 20(4), 537–549, doi:10.1016/j.neunet.2007.04.024.

551 Chen, C. (2007), A finite smoothing algorithm for quantile regression, *Journal of Computational*
552 *and Graphical Statistics*, 16(1), 136–164, doi:10.1198/106186007X180336.

553 Chernozhukov, V., I. Fernández-Val, and A. Galichon (2010), Quantile and probability curves
554 without crossing, *Econometrica*, 78(3), 1093–1125, doi:10.3982/ECTA7880.

555 Doksum, K., and J.-Y. Koo (2000), On spline estimators and prediction intervals in nonparamet-
556 ric regression, *Computational Statistics & Data Analysis*, 35(1), 67–82, doi:10.1016/S0167-
557 9473(99)00116-4.

558 Environment and Climate Change Canada (2014), *Intensity-Duration-Frequency (IDF) Files*
559 *v2.30.*

560 Friederichs, P., and A. Hense (2007), Statistical downscaling of extreme precipitation events
561 using censored quantile regression, *Monthly Weather Review*, 135(6), 2365–2378, doi:
562 10.1175/MWR3403.1.

563 Hanson, S. J., and D. J. Burr (1988), Minkowski-r back-propagation: Learning in connectionist
564 models with non-Euclidian error signals, in *Neural Information Processing Systems*, pp. 348–
565 357.

566 Hirschi, M., S. I. Seneviratne, V. Alexandrov, F. Boberg, C. Boroneant, O. B. Christensen,
567 H. Formayer, B. Orłowsky, and P. Stepanek (2010), Observational evidence for soil-moisture
568 impact on hot extremes in southeastern Europe, *Nature Geoscience*, 4(1), ngeo1032, doi:
569 10.1038/ngeo1032.

570 Hofmeister, T. (2017), *qrsvm: SVM Quantile Regression with the Pinball Loss*, R package version
571 0.2.1.

572 Huber, P. J. (1964), Robust estimation of a location parameter, *The Annals of Mathematical Statis-*
573 *tics*, 35(1), 73–101.

574 Jiang, C., M. Jiang, Q. Xu, and X. Huang (2017), Expectile regression neural network model with
575 applications, *Neurocomputing*, 247, 73–86, doi:10.1016/j.neucom.2017.03.040.

576 Jiang, X., J. Jiang, and X. Song (2012), Oracle model selection for nonlinear models
577 based on weighted composite quantile regression, *Statistica Sinica*, pp. 1479–1506, doi:
578 10.5705/ss.2010.203.

579 Karatzoglou, A., A. Smola, K. Hornik, and A. Zeileis (2004), kernlab – an S4 package for kernel
580 methods in R, *Journal of Statistical Software*, 11(9), 1–20.

581 Koenker, R., and G. Bassett Jr. (1978), Regression quantiles, *Econometrica: Journal of the Econo-*
582 *metric Society*, pp. 33–50.

583 Koenker, R., and F. Schorfheide (1994), Quantile spline models for global temperature change,
584 *Climatic Change*, 28(4), 395–404, doi:10.1007/BF01104081.

585 Kuo, C.-C., T. Y. Gan, and S. Chan (2012), Regional intensity-duration-frequency curves derived
586 from ensemble empirical mode decomposition and scaling property, *Journal of Hydrologic En-*
587 *gineering*, 18(1), 66–74, doi:10.1061/(ASCE)HE.1943-5584.0000612.

- 588 Lang, B. (2005), Monotonic multi-layer perceptron networks as universal approximators, *Artifi-*
589 *cial Neural Networks: Formal Models and Their Applications–ICANN 2005*, pp. 31–37, doi:
590 10.1007/11550907_6.
- 591 Liu, Y., and Y. Wu (2009), Stepwise multiple quantile regression estimation using non-crossing
592 constraints, *Statistics and its Interface*, 2(3), 299–310, doi:10.4310/SII.2009.v2.n3.a4.
- 593 Liu, Y., and Y. Wu (2011), Simultaneous multiple non-crossing quantile regression estima-
594 tion using kernel constraints, *Journal of Nonparametric Statistics*, 23(2), 415–437, doi:
595 10.1080/10485252.2010.537336.
- 596 Madsen, H., I. B. Gregersen, D. Rosbjerg, and K. Arnbjerg-Nielsen (2017), Regional frequency
597 analysis of short duration rainfall extremes using gridded daily rainfall data as co-variate, *Water*
598 *Science and Technology*, 75(8), 1971–1981, doi:10.2166/wst.2017.089.
- 599 Mailhot, A., S. Lachance-Cloutier, G. Talbot, and A.-C. Favre (2013), Regional estimates of in-
600 tense rainfall based on the Peak-Over-Threshold (POT) approach, *Journal of Hydrology*, 476,
601 188–199, doi:10.1016/j.jhydrol.2012.10.036.
- 602 McKenney, D. W., M. F. Hutchinson, P. Papadopol, K. Lawrence, J. Pedlar, K. Campbell,
603 E. Milewska, R. F. Hopkinson, D. Price, and T. Owen (2011), Customized spatial climate mod-
604 els for North America, *Bulletin of the American Meteorological Society*, 92(12), 1611–1622,
605 doi:10.1175/2011BAMS3132.1.
- 606 Minin, A., M. Velikova, B. Lang, and H. Daniels (2010), Comparison of universal approxima-
607 tors incorporating partial monotonicity by structure, *Neural Networks*, 23(4), 471–475, doi:
608 10.1016/j.neunet.2009.09.002.
- 609 Muggeo, V. M., M. Sciandra, and L. Augugliaro (2012), Quantile regression via iterative least
610 squares computations, *Journal of Statistical Computation and Simulation*, 82(11), 1557–1569,
611 doi:10.1080/00949655.2011.583650.

- 612 Muggeo, V. M., M. Sciandra, A. Tomasello, and S. Calvo (2013), Estimating growth charts via
613 nonparametric quantile regression: a practical framework with application in ecology, *Environ-*
614 *mental and Ecological Statistics*, 20(4), 519–531, doi:10.1007/s10651-012-0232-1.
- 615 Newey, W. K., and J. L. Powell (1987), Asymmetric least squares estimation and testing, *Econo-*
616 *metrica*, pp. 819–847.
- 617 Ouali, D., and A. J. Cannon (2017), Estimation of rainfall Intensity-Duration-Frequency curves at
618 ungauged locations using quantile regression methods, *Stochastic Environmental Research and*
619 *Risk Assessment*.
- 620 Ouali, D., F. Chebana, and T. Ouarda (2016), Quantile regression in regional frequency analysis:
621 A better exploitation of the available information, *Journal of Hydrometeorology*, 17(6), 1869–
622 1883, doi:10.1175/JHM-D-15-0187.1.
- 623 Ouali, D., F. Chebana, and T. Ouarda (2017), Fully nonlinear statistical and machine-learning
624 approaches for hydrological frequency estimation at ungauged sites, *Journal of Advances in*
625 *Modeling Earth Systems*, 9(2), 1292–1306, doi:10.1002/2016MS000830.
- 626 Ouarda, T. B., C. Girard, G. S. Cavadias, and B. Bobée (2001), Regional flood frequency estimation
627 with canonical correlation analysis, *Journal of Hydrology*, 254(1), 157–173, doi:10.1016/S0022-
628 1694(01)00488-7.
- 629 Plate, T. A. (1999), Accuracy versus interpretability in flexible modeling: Implementing a tradeoff
630 using Gaussian process models, *Behaviormetrika*, 26(1), 29–50.
- 631 Potts, W. J. (1999), Generalized additive neural networks, in *Proceedings of the Fifth ACM*
632 *SIGKDD International Conference on Knowledge Discovery and Data Mining*, pp. 194–200,
633 ACM.
- 634 Quiñonero Candela, J., C. E. Rasmussen, F. Sinz, O. Bousquet, and B. Schölkopf (2006), Eval-

635 uating predictive uncertainty challenge, *Lecture Notes in Computer Science*, 3944, 1–27, doi:
636 10.1007/11736790_1.

637 Roth, M., T. Buishand, and G. Jongbloed (2015), Trends in moderate rainfall extremes: A regional
638 monotone regression approach, *Journal of Climate*, 28(22), 8760–8769, doi:10.1175/JCLI-D-
639 14-00685.1.

640 Saito, H., D. Nakayama, and H. Matsuyama (2010), Relationship between the initiation of a shal-
641 low landslide and rainfall intensity-duration thresholds in Japan, *Geomorphology*, 118(1), 167–
642 175, doi:10.1016/j.geomorph.2009.12.016.

643 Shephard, M. W., E. Mekis, R. J. Morris, Y. Feng, X. Zhang, K. Kilcup, and R. Fleetwood (2014),
644 Trends in Canadian short-duration extreme rainfall: Including an Intensity–Duration–Frequency
645 perspective, *Atmosphere-Ocean*, 52(5), 398–417, doi:10.1080/07055900.2014.969677.

646 Sun, J., Y. Gai, and L. Lin (2013), Weighted local linear composite quantile estimation for the case
647 of general error distributions, *Journal of Statistical Planning and Inference*, 143(6), 1049–1063,
648 doi:10.1016/j.jspi.2013.01.002.

649 Takeuchi, I., Q. V. Le, T. D. Sears, and A. J. Smola (2006), Nonparametric quantile estimation,
650 *Journal of Machine Learning Research*, 7(Jul), 1231–1264.

651 Taylor, J. W. (2000), A quantile regression neural network approach to estimating the condi-
652 tional density of multiperiod returns, *Journal of Forecasting*, 19(4), 299–311, doi:10.1002/1099-
653 131X(200007)19:4<299::AID-FOR775>3.0.CO;2-V.

654 Waltrup, L. S., F. Sobotka, T. Kneib, and G. Kauermann (2015), Expectile and quantile regression–
655 David and Goliath?, *Statistical Modelling*, 15(5), 433–456, doi:10.1177/1471082X14561155.

656 Wasko, C., and A. Sharma (2014), Quantile regression for investigating scaling of ex-
657 treme precipitation with temperature, *Water Resources Research*, 50(4), 3608–3614, doi:
658 10.1002/2013WR015194.

- 659 White, H. (1992), Nonparametric estimation of conditional quantiles using neural networks, in
660 *Computing Science and Statistics*, edited by C. Page and R. LePage, pp. 190–199, Springer,
661 doi:10.1007/978-1-4612-2856-1_25.
- 662 Xu, Q., K. Deng, C. Jiang, F. Sun, and X. Huang (2017), Composite quantile regression
663 neural network with applications, *Expert Systems with Applications*, 76, 129–139, doi:
664 10.1016/j.eswa.2017.01.054.
- 665 Yao, Q., and H. Tong (1996), Asymmetric least squares regression estimation: A
666 nonparametric approach, *Journal of Nonparametric Statistics*, 6(2-3), 273–292, doi:
667 10.1080/10485259608832675.
- 668 Zhang, H., and Z. Zhang (1999), Feedforward networks with monotone constraints, in *IJCNN'99*,
669 *International Joint Conference on Neural Networks*, vol. 3, pp. 1820–1823, IEEE, doi:
670 10.1109/IJCNN.1999.832655.
- 671 Zou, H., and M. Yuan (2008), Composite quantile regression and the oracle model selection theory,
672 *The Annals of Statistics*, pp. 1108–1126, doi:10.1214/07-AOS507.

673 List of Figures

674	1	Predictions from QRNN (panels a and c) and MCQRNN (panels b and d) models	
675		fit to synthetic data (black points) generated by equation 14 (panels a and b) and	
676		equation 15 (panels c and d) are shown in rainbow colours. Plots of the true con-	
677		ditional quantile functions are shown by solid grey lines. The nine curves from	
678		bottom to top represent $\tau = 0.1, 0.2, \dots, 0.9$	34
679	2	As in Figures 1b and 1d, but for MCQRNN models with additional (a) positivity	
680		constraints and (b) positivity and monotonicity constraints, respectively. (c, d)	
681		Estimates of 95% confidence intervals, based on 500 parametric bootstrap datasets,	
682		for the $\tau = 0.1, 0.5, 0.9$ -quantile regression curves shown in Figures 1b and 1d. . .	35
683	3	Distribution of RMSE ranks from 1st (or best) in dark grey to 4th (or worst) in	
684		light grey for MLP, QRNN, CQRNN, and MCQRNN models over 1000 Monte	
685		Carlo simulations for examples 1, 2, and 3 from <i>Xu et al.</i> (2017) with $N(0, 0.25)$	
686		(rnorm25), $t(3)$ (rt3), and $\chi^2(3)$ (rchisq3) distributed noise.	36
687	4	Example ECCC IDF data for Victoria Intl A (station 1018621) in British Columbia,	
688		Canada. Points (\times) show quantiles associated with 2-yr, 5-yr, 10-yr, 25-yr, 50-yr,	
689		and 100-yr (from bottom to top) return period intensities estimated by fitting the	
690		Gumbel distribution by the method of moments to annual maximum rainfall rate	
691		data for 5-, 10-, 15-, 30-, 60-min, 2-, 6-, 12-, and 24-hr durations (left to right).	
692		Lines are from best fit linear interpolation equations between log-transformed du-	
693		ration and log-transformed Gumbel quantiles for each return period.	37
694	5	Points (\bullet) show locations of ECCC IDF curve stations; point size is proportional to	
695		station elevation. Shading indicates the climatological summer total precipitation	
696		(1971-2000).	38
697	6	Leave-one-out predictions of IDF curves for 2-yr, 5-yr, 10-yr, 25-yr, 50-yr, and	
698		100-yr (in rainbow colours from bottom to top) return period intensities for Victo-	
699		ria Intl A (station 1018621) from (a) QRNN models and (b) MCQRNN model (cf.	
700		Figure 4). Points (\blacksquare) show observed annual maximum rainfall rate data for 5-, 10-,	
701		15-, 30-, 60-min, 2-, 6-, 12-, and 24-hr durations.	39
702	7	Cross-validated relative differences RD_τ (%) in quantile regression error between	
703		MCQRNN and QRNN IDF curve predictions for $J = 1, 2, \dots, 5$ using QRNN ($J =$	
704		1) as the reference model. Results are shown for 2-yr, 5-yr, 10-yr, 25-yr, 50-yr, and	
705		100-yr return periods.	40
706	8	Mean quantile regression error ratio R_τ between at-site ECCC IDF curves and	
707		leave-one-out cross-validated MCQRNN predictions; values of R_τ are stratified	
708		according to the median distance between the left-out station and its 80 neighbour-	
709		ing stations. Each of the 10 distance groupings contains an approximately equal	
710		numbers of stations (56 or 57).	41
711	9	Schematic representations of (a) the generalized additive neural network architec-	
712		ture from <i>Potts</i> (1999) and (b) additivity constraints applied to a fully-connected	
713		MLP via a binary mask $\mathbf{A}^{(h)}$ applied to elements of $\mathbf{W}^{(h)}$. Parameters that have	
714		been set to zero by $\mathbf{A}^{(h)}$ are represented by dashed grey lines. Nonzero $\mathbf{W}^{(h)}$, \mathbf{w}	
715		parameters are represented by solid coloured lines, $\mathbf{b}^{(h)}$ parameters by dashed	
716		coloured lines, and b by dashed black lines.	42

717	10	Modified generalized additive model plots (<i>Plate</i> , 1999) for covariates x_1 , x_2 , x_3 , and x_4 from MLP models ($\lambda^{(h)} = 0, 0.2, 1, 100$) fit to synthetic data generated by equation 25. The vertical axis shows partial effects for each predictor.	43
718			
719	11	(a) Interaction strength for covariates x_1 , x_2 , x_3 , and x_4 (<i>Plate</i> , 1999), (b) training and testing RMSE, and (c) absolute magnitudes of $\mathbf{W}^{(h)}$ elements (cf. equation 24) associated with different values of $\lambda^{(h)}$	44
720			
721			
722			

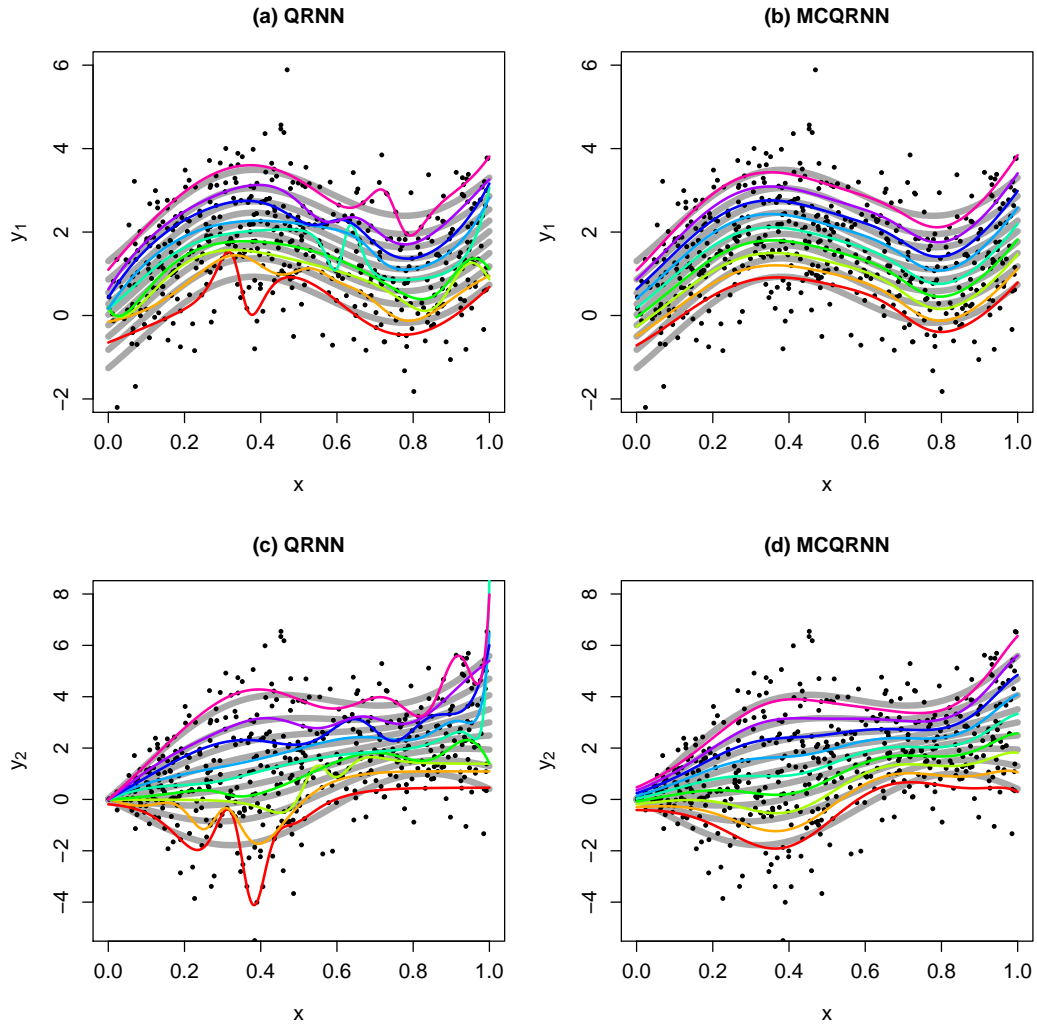


Figure 1: Predictions from QRNN (panels a and c) and MCQRNN (panels b and d) models fit to synthetic data (black points) generated by equation 14 (panels a and b) and equation 15 (panels c and d) are shown in rainbow colours. Plots of the true conditional quantile functions are shown by solid grey lines. The nine curves from bottom to top represent $\tau = 0.1, 0.2, \dots, 0.9$.

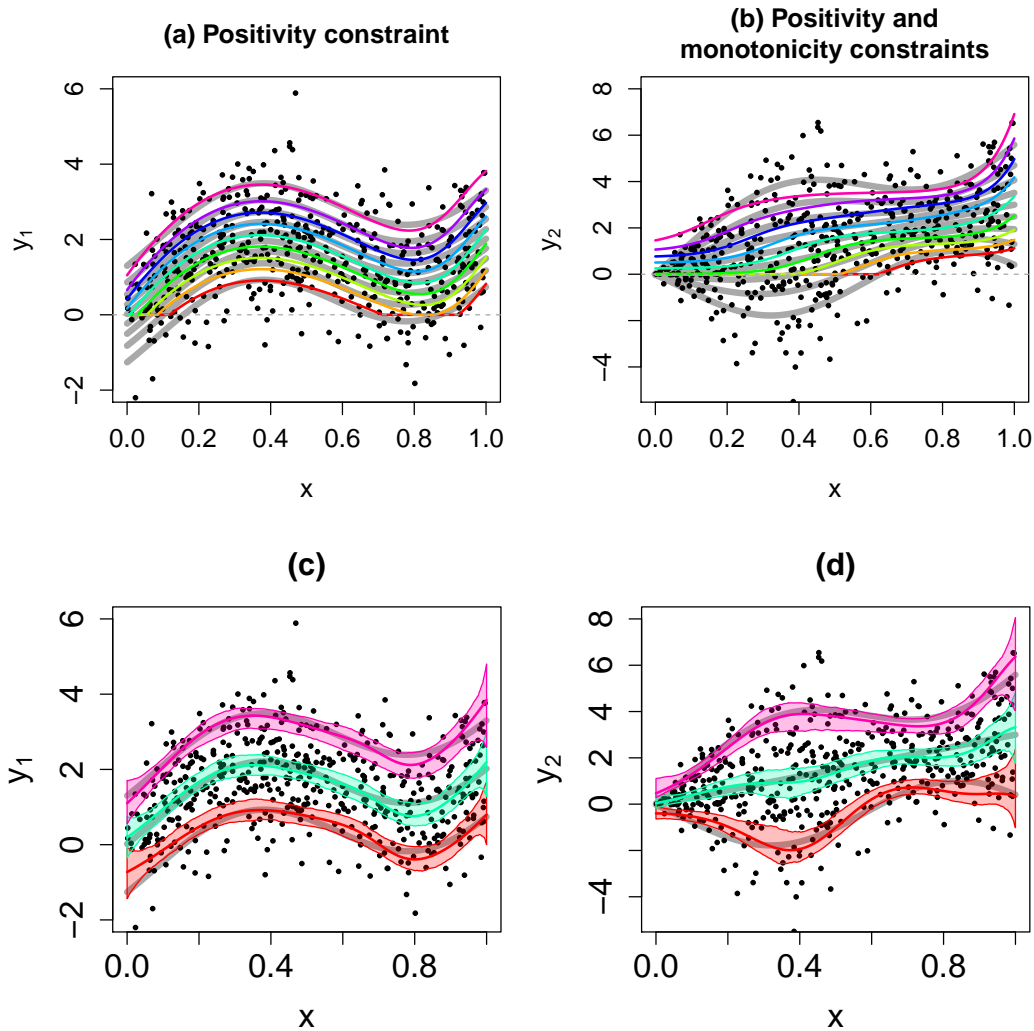


Figure 2: As in Figures 1b and 1d, but for MCQRNN models with additional (a) positivity constraints and (b) positivity and monotonicity constraints, respectively. (c, d) Estimates of 95% confidence intervals, based on 500 parametric bootstrap datasets, for the $\tau = 0.1, 0.5, 0.9$ -quantile regression curves shown in Figures 1b and 1d.

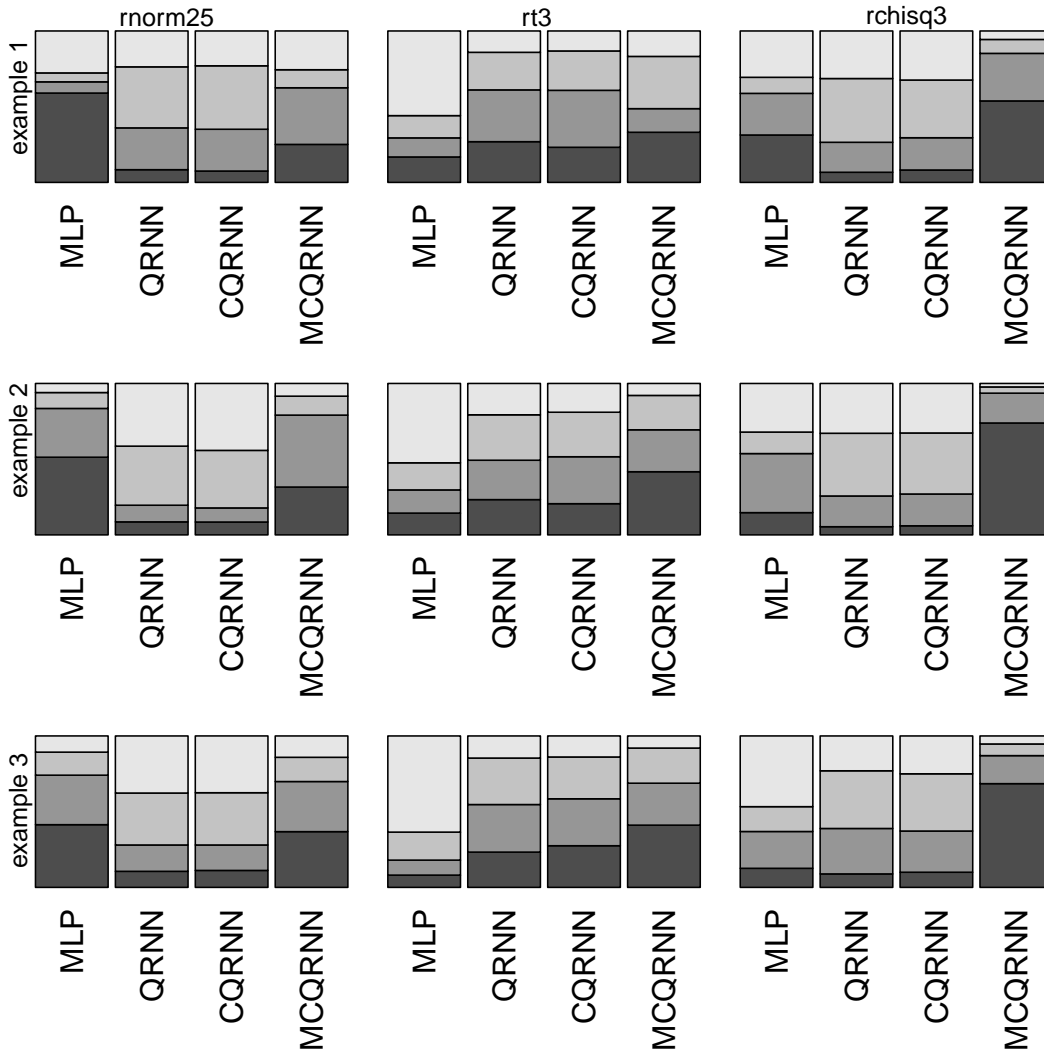


Figure 3: Distribution of RMSE ranks from 1st (or best) in dark grey to 4th (or worst) in light grey for MLP, QRNN, CQRNN, and MCQRNN models over 1000 Monte Carlo simulations for examples 1, 2, and 3 from *Xu et al. (2017)* with $N(0, 0.25)$ (rnorm25), $t(3)$ (rt3), and $\chi^2(3)$ (rchisq3) distributed noise.

Short Duration Rainfall Intensity–Duration–Frequency Data

2014/12/21

Données sur l'intensité, la durée et la fréquence des chutes de pluie de courte durée

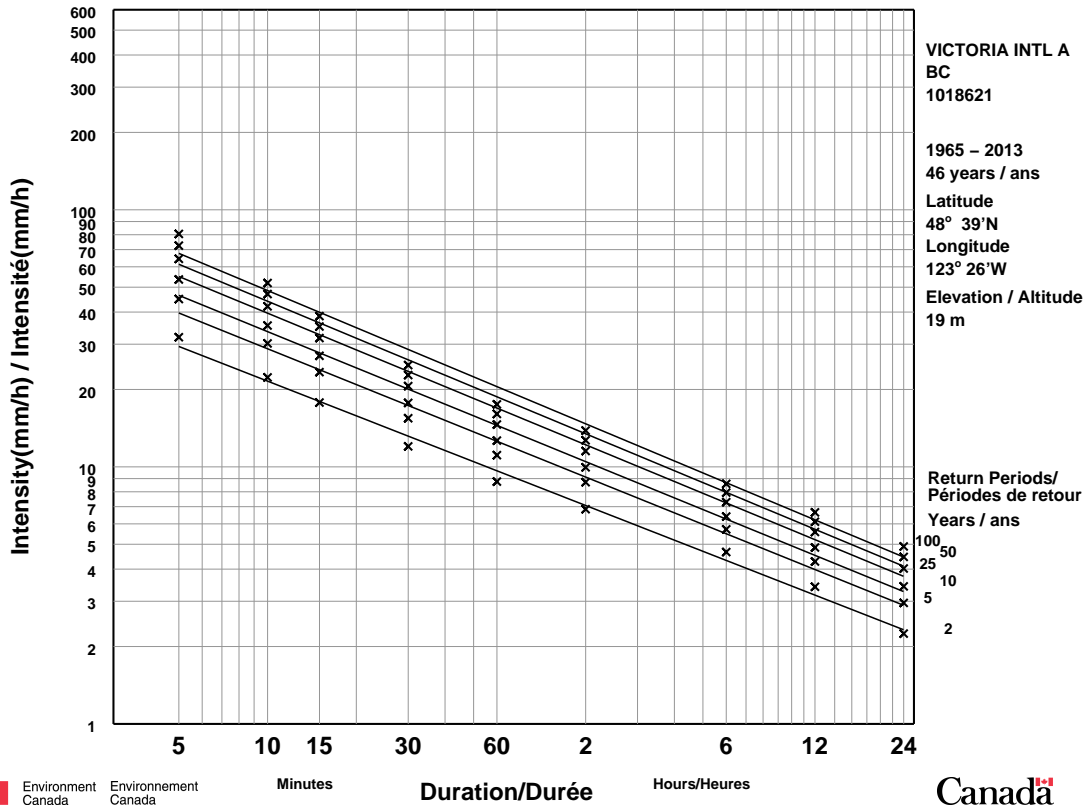


Figure 4: Example ECCC IDF data for Victoria Intl A (station 1018621) in British Columbia, Canada. Points (×) show quantiles associated with 2-yr, 5-yr, 10-yr, 25-yr, 50-yr, and 100-yr (from bottom to top) return period intensities estimated by fitting the Gumbel distribution by the method of moments to annual maximum rainfall rate data for 5-, 10-, 15-, 30-, 60-min, 2-, 6-, 12-, and 24-hr durations (left to right). Lines are from best fit linear interpolation equations between log-transformed duration and log-transformed Gumbel quantiles for each return period.

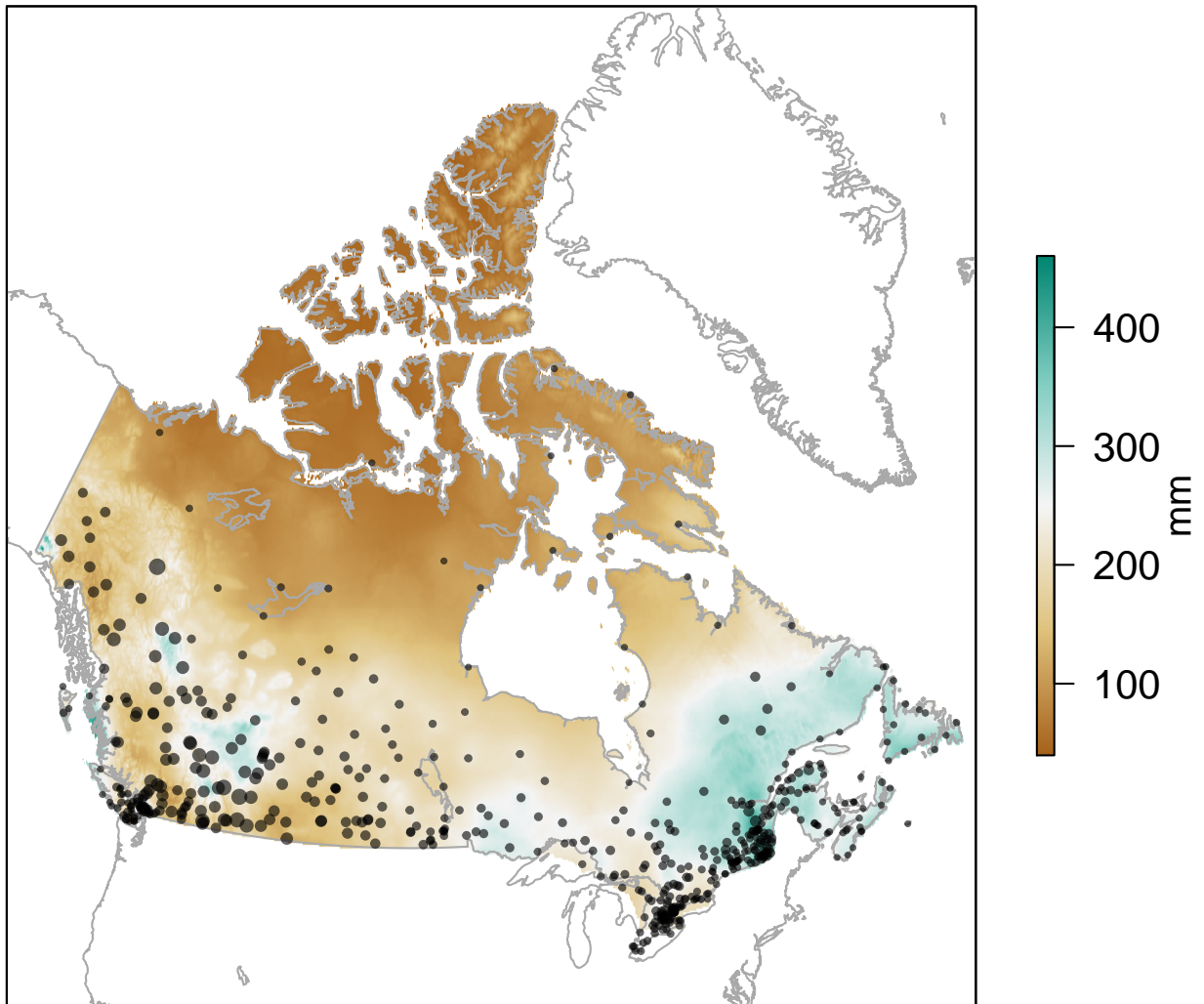


Figure 5: Points (●) show locations of ECCC IDF curve stations; point size is proportional to station elevation. Shading indicates the climatological summer total precipitation (1971-2000).

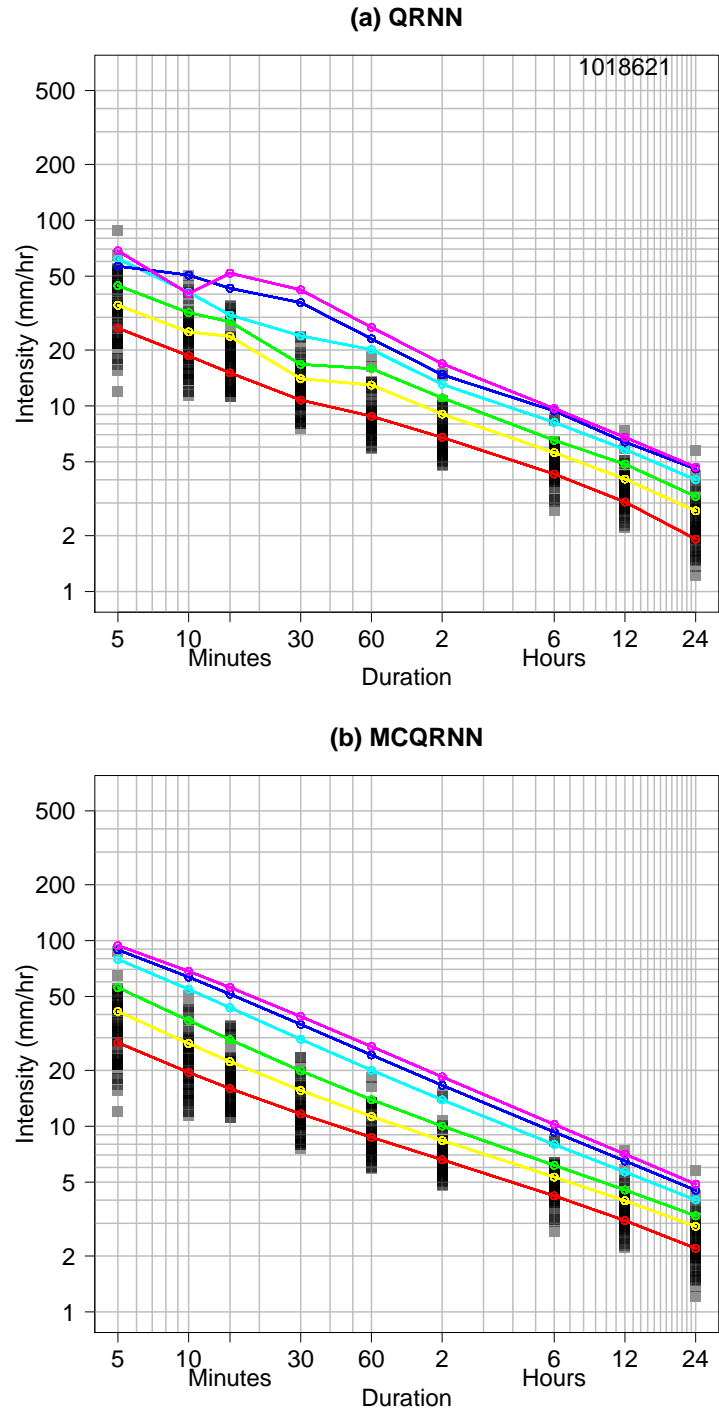


Figure 6: Leave-one-out predictions of IDF curves for 2-yr, 5-yr, 10-yr, 25-yr, 50-yr, and 100-yr (in rainbow colours from bottom to top) return period intensities for Victoria Intl A (station 1018621) from (a) QRNN models and (b) MCQRNN model (cf. Figure 4). Points (■) show observed annual maximum rainfall rate data for 5-, 10-, 15-, 30-, 60-min, 2-, 6-, 12-, and 24-hr durations.

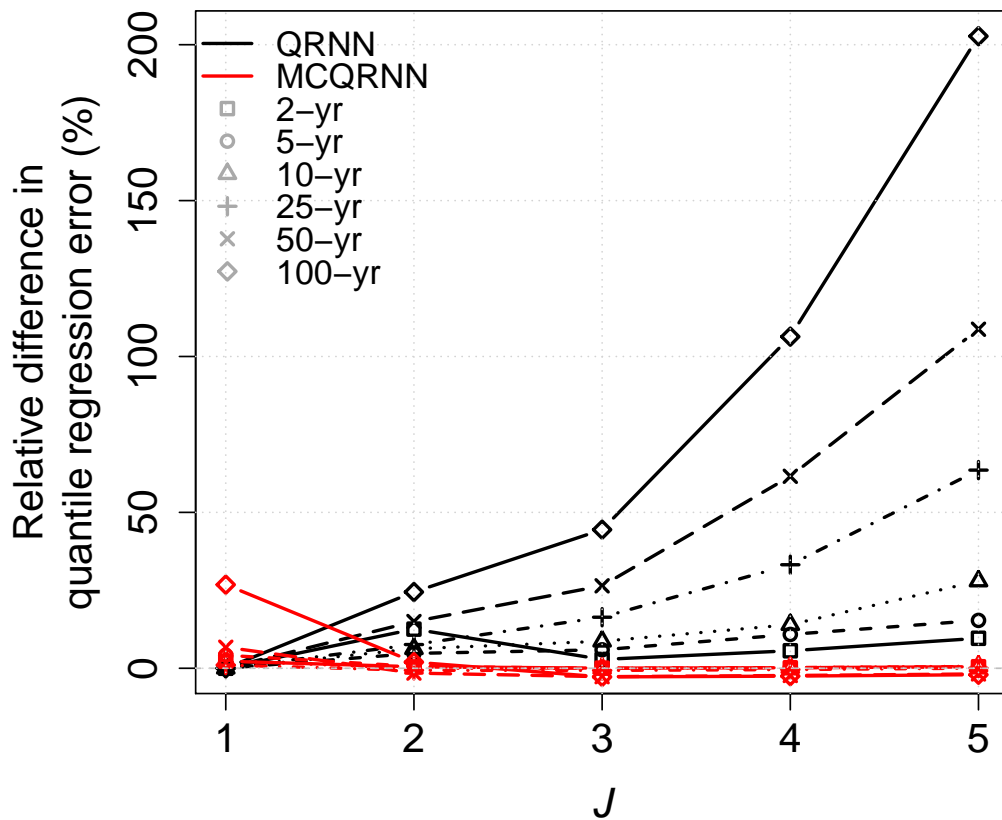


Figure 7: Cross-validated relative differences RD_{τ} (%) in quantile regression error between MC-QRNN and QRNN IDF curve predictions for $J = 1, 2, \dots, 5$ using QRNN ($J = 1$) as the reference model. Results are shown for 2-yr, 5-yr, 10-yr, 25-yr, 50-yr, and 100-yr return periods.

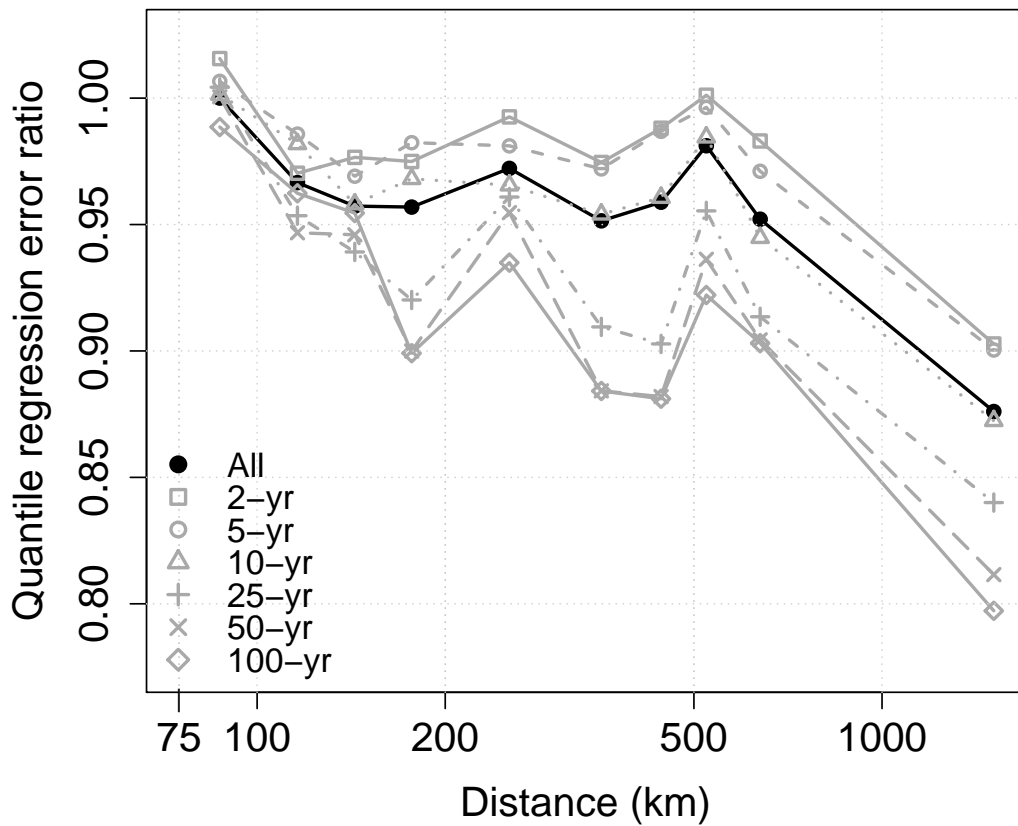


Figure 8: Mean quantile regression error ratio R_τ between at-site ECCC IDF curves and leave-one-out cross-validated MCQRNN predictions; values of R_τ are stratified according to the median distance between the left-out station and its 80 neighbouring stations. Each of the 10 distance groupings contains an approximately equal numbers of stations (56 or 57).

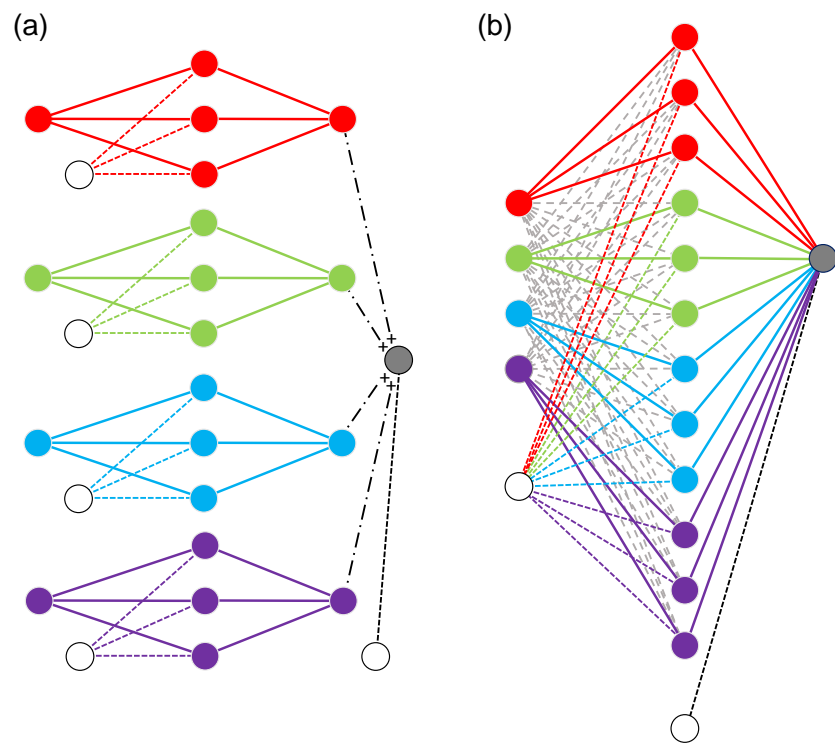


Figure 9: Schematic representations of (a) the generalized additive neural network architecture from *Potts* (1999) and (b) additivity constraints applied to a fully-connected MLP via a binary mask $\mathbf{A}^{(h)}$ applied to elements of $\mathbf{W}^{(h)}$. Parameters that have been set to zero by $\mathbf{A}^{(h)}$ are represented by dashed grey lines. Nonzero $\mathbf{W}^{(h)}$, \mathbf{w} parameters are represented by solid coloured lines, $\mathbf{b}^{(h)}$ parameters by dashed coloured lines, and b by dashed black lines.

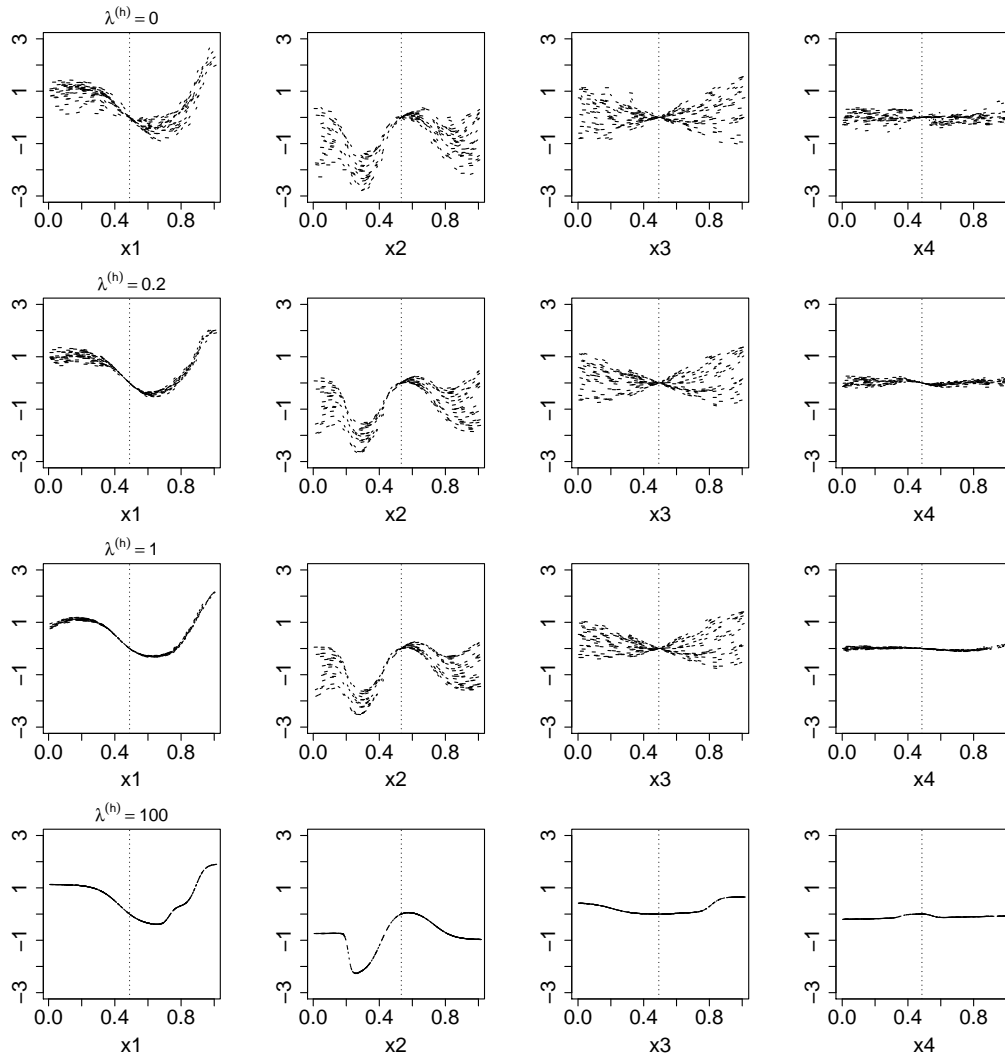


Figure 10: Modified generalized additive model plots (*Plate, 1999*) for covariates $x_1, x_2, x_3,$ and x_4 from MLP models ($\lambda^{(h)} = 0, 0.2, 1, 100$) fit to synthetic data generated by equation 25. The vertical axis shows partial effects for each predictor.

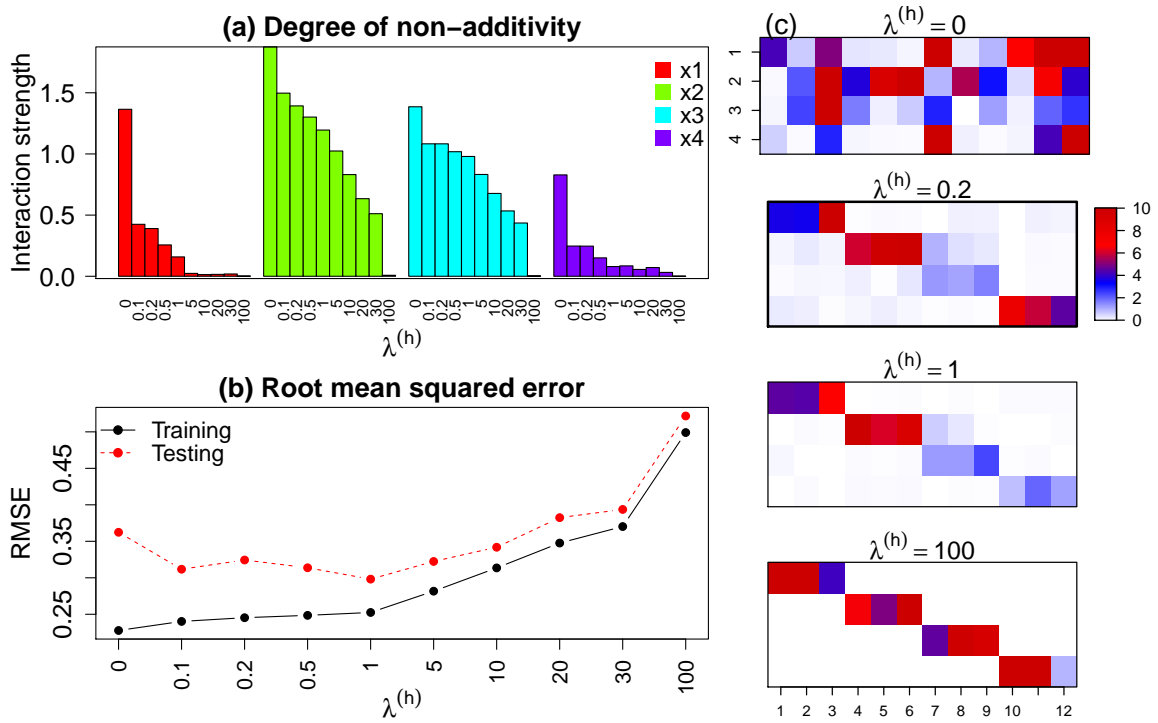


Figure 11: (a) Interaction strength for covariates x_1 , x_2 , x_3 , and x_4 (Plate, 1999), (b) training and testing RMSE, and (c) absolute magnitudes of $\mathbf{W}^{(h)}$ elements (cf. equation 24) associated with different values of $\lambda^{(h)}$.

723 **List of Tables**

724 1 Summary of RMSE values for MLP, QRNN, CQRNN, and MCQRNN models
 725 based on Monte Carlo simulations for examples 1, 2, and 3 from *Xu et al. (2017)*
 726 with normal $N(0, 0.25)$ (rnorm25), $t(3)$ (rt3), and $\chi^2(3)$ (rchisq3) distributed noise.
 727 The first value in each column is the median over 1000 simulations; values in
 728 parentheses are 5th and 95th percentiles. Bold (underlined) values in each row
 729 indicate the best (worst) performing model for the median, 5th, and 95th percentiles. 46

730 2 Summary of cross-validated relative differences RD_τ (%) in quantile regression
 731 error stratified by duration D , for all stations, for MCQRNN models (a) without
 732 weighting and (b) with weighting proportional to $\log(D)$. In both cases, QRNN
 733 IDF curve predictions serve as the reference model. Bold values indicate combi-
 734 nations of return period and duration for which MCQRNN performs better (i.e.,
 735 lower errors) than QRNN; combinations with worse performance are underlined. . 47

736 3 Summary of quantile regression error ratio R_τ stratified by duration D between at-
 737 site ECCC IDF curves and ungauged MCQRNN predictions for all stations. Values
 738 ≥ 0.9 are shown in bold. 48

Table 1: Summary of RMSE values for MLP, QRNN, CQRNN, and MCQRNN models based on Monte Carlo simulations for examples 1, 2, and 3 from *Xu et al. (2017)* with normal $N(0, 0.25)$ (rnorm25), $t(3)$ (rt3), and $\chi^2(3)$ (rchisq3) distributed noise. The first value in each column is the median over 1000 simulations; values in parentheses are 5th and 95th percentiles. Bold (underlined) values in each row indicate the best (worst) performing model for the median, 5th, and 95th percentiles.

Dataset	MLP	QRNN	CQRNN	MCQRNN
example 1 (rnorm25)	0.182 (0.143, 0.266)	0.185 (0.141, 0.301)	0.185 (0.141, 0.298)	0.181 (0.139, 0.289)
example 1 (rt3)	<u>0.878 (0.733, 1.29)</u>	0.852 (0.715, 1.13)	0.852 (0.716, 1.12)	0.853 (0.722, 1.10)
example 1 (rchisq3)	1.34 (1.16, <u>1.65</u>)	<u>1.35 (1.17, 1.57)</u>	<u>1.35 (1.17, 1.57)</u>	1.31 (1.13, 1.50)
example 2 (rnorm25)	0.057 (0.051, 0.064)	<u>0.059 (0.052, 0.068)</u>	<u>0.059 (0.052, 0.067)</u>	0.057 (0.051, 0.065)
example 2 (rt3)	<u>0.383 (0.304, 12.9)</u>	0.367 (0.297, 0.565)	0.365 (0.295, 0.548)	0.361 (0.294, 0.515)
example 2 (rchisq3)	<u>0.584 (0.477, 12.9)</u>	0.582 (0.479, 0.744)	0.583 (<u>0.482</u> , 0.750)	0.553 (0.458, 0.677)
example 3 (rnorm25)	0.274 (0.251, 0.301)	<u>0.283 (0.257, 0.319)</u>	<u>0.283 (0.257, 0.320)</u>	0.275 (0.250 , 0.303)
example 3 (rt3)	<u>1.95 (1.51, 576)</u>	1.76 (1.46, 6.37)	1.75 (1.46, 5.78)	1.73 (1.45, 3.49)
example 3 (rchisq3)	<u>2.82 (2.37, 1359)</u>	2.73 (2.35, 16.9)	2.73 (2.35, 24.6)	2.60 (2.24, 4.69)

Table 2: Summary of cross-validated relative differences RD_τ (%) in quantile regression error stratified by duration D , for all stations, for MCQRNN models (a) without weighting and (b) with weighting proportional to $\log(D)$. In both cases, QRNN IDF curve predictions serve as the reference model. Bold values indicate combinations of return period and duration for which MCQRNN performs better (i.e., lower errors) than QRNN; combinations with worse performance are underlined.

(a) Unweighted

Return period / Duration	5-min	10-min	15-min	30-min	60-min	2-hr	6-hr	12-hr	24-hr
2	-0.1	-0.2	0	<u>+0.1</u>	-0.1	+0.4	<u>+1.5</u>	<u>+2.7</u>	<u>+4.8</u>
5	-0.1	<u>+0.2</u>	<u>+0.3</u>	-0.6	-0.4	-0.3	<u>+1.0</u>	<u>+0.5</u>	<u>+1.9</u>
10	<u>+0.2</u>	<u>+0.1</u>	<u>+0.2</u>	-0.8	-0.6	-0.8	<u>+0.7</u>	<u>+1.8</u>	<u>+1.7</u>
25	<u>+0.2</u>	-1.0	-1.4	-1.1	-1.6	-1.4	<u>+1.1</u>	<u>+0.3</u>	<u>+0.6</u>
50	-2.1	-3.5	-3.9	-1.9	-1.1	-6.7	<u>+0.9</u>	<u>+0.8</u>	<u>+2.9</u>
100	-4.0	-2.4	-4.6	-4.7	<u>+1.6</u>	<u>+0.9</u>	<u>+2.8</u>	<u>+4.3</u>	<u>+5.6</u>

(b) $\log(D)$ weighting

Return period / Duration	5-min	10-min	15-min	30-min	60-min	2-hr	6-hr	12-hr	24-hr
2	<u>+0.3</u>	-0.3	-0.1	0	-0.3	-0.3	<u>+0.2</u>	<u>+1.3</u>	<u>+2.9</u>
5	<u>+0.2</u>	<u>+0.2</u>	<u>+0.3</u>	-0.7	-0.6	-0.7	<u>+0.1</u>	-0.2	<u>+1.1</u>
10	0	-0.1	<u>+0.1</u>	-0.9	-0.8	-1.0	-0.1	<u>+1.0</u>	<u>+0.9</u>
25	<u>+0.1</u>	-1.0	-1.6	-1.3	-1.5	-1.6	<u>+0.3</u>	-0.8	-0.8
50	-2.1	-3.6	-4.1	-2.4	-1.4	-7.0	<u>+0.1</u>	-0.8	<u>+0.7</u>
100	-3.3	-2.5	-5.0	-5.6	<u>+0.6</u>	<u>+0.3</u>	<u>+1.6</u>	<u>+1.7</u>	<u>+1.9</u>

Table 3: Summary of quantile regression error ratio R_τ stratified by duration D between at-site ECCC IDF curves and ungauged MCQRNN predictions for all stations. Values ≥ 0.9 are shown in bold.

Return period / Duration	5-min	10-min	15-min	30-min	60-min	2-hr	6-hr	12-hr	24-hr
2	1.05	0.97	0.98	0.99	0.99	0.98	0.95	0.94	0.97
5	1.06	0.96	0.97	0.99	0.99	0.98	0.94	0.93	0.95
10	1.05	0.94	0.95	0.99	0.99	0.97	0.92	0.90	0.93
25	1.03	0.91	0.91	0.99	0.98	0.97	0.89	0.85	0.88
50	1.02	0.90	0.89	0.95	0.97	0.95	0.86	0.79	0.84
100	0.99	0.87	0.85	0.89	0.94	0.91	0.78	0.74	0.78